

LEAD REMOVAL FROM WATER BY MODIFIED ACTIVATED CARBON PRODUCED FROM  
BANANA STEM



A Thesis Submitted in Partial Fulfillment of the Requirements  
for the Degree of Master of Science in Green Chemistry and Sustainability

Department of Chemistry

FACULTY OF SCIENCE

Chulalongkorn University

Academic Year 2022

Copyright of Chulalongkorn University

การกำจัดตะกั่วจากน้ำด้วยคาร์บอนกัมมันต์ดัดแปรที่ผลิตจากลำต้นกล้วย



วิทยานิพนธ์นี้เป็นส่วนหนึ่งของการศึกษาตามหลักสูตรปริญญาวิทยาศาสตรมหาบัณฑิต  
สาขาวิชาเคมีสีเขียวและความยั่งยืน ภาควิชาเคมี  
คณะวิทยาศาสตร์ จุฬาลงกรณ์มหาวิทยาลัย  
ปีการศึกษา 2565  
ลิขสิทธิ์ของจุฬาลงกรณ์มหาวิทยาลัย

Thesis Title	LEAD REMOVAL FROM WATER BY MODIFIED ACTIVATED CARBON PRODUCED FROM BANANA STEM
By	Miss Imelda Octa Tampubolon
Field of Study	Green Chemistry and Sustainability
Thesis Advisor	Assistant Professor Numpon Insin, Ph.D.

---

Accepted by the FACULTY OF SCIENCE, Chulalongkorn University in Partial Fulfillment of the Requirement for the Master of Science

..... Dean of the FACULTY OF SCIENCE  
(Professor POLKIT SANGVANICH, Ph.D.)

THESIS COMMITTEE

..... Chairman  
(Associate Professor Dr. FUANGFA UNOB)

..... Thesis Advisor  
(Assistant Professor Numpon Insin, Ph.D.)

..... External Examiner  
(Dr. Samerkhae Jongthammanurak)

จุฬาลงกรณ์มหาวิทยาลัย  
CHULALONGKORN UNIVERSITY

อิมเลตา ออกตา แคมป์โบลอน : การกำจัดตะกั่วจากน้ำด้วยคาร์บอนกัมมันต์ดัดแปรที่ผลิตจากลำต้นกล้วย. ( LEAD REMOVAL FROM WATER BY MODIFIED ACTIVATED CARBON PRODUCED FROM BANANA STEM) อ.ที่ปรึกษาหลัก : นำพล อินสิน

ถ่านกัมมันต์จากต้นกล้วย (BSAC) และถ่านกัมมันต์จากต้นกล้วยที่ถูกดัดแปรจะประกอบด้วยธาตุกำมะถัน ไนโตรเจน และออกซิเจน ที่ได้จากการเผาต้นกล้วยซึ่งได้ทำการเตรียมและศึกษาการกำจัดไอออนตะกั่ว Pb(II) วัสดุดังกล่าวถูกวิเคราะห์ด้วยกล้องจุลทรรศน์อิเล็กตรอนแบบส่องกราด, การเลี้ยวเบนของรังสีเอกซ์ การวิเคราะห์พื้นที่ผิวและฟูเรียร์ทรานส์ฟอร์มอินฟราเรดสเปกโทรสโกปี ผลจากภาพถ่ายด้วยกล้องจุลทรรศน์ อิเล็กตรอนแบบส่องกราดแสดงให้เห็นว่าวัสดุมีรูพรุน และการเลี้ยวเบนของรังสีเอกซ์ยืนยันได้ว่าโครงสร้างที่ได้มีลักษณะอสัณฐานและกับโครงสร้างหกเหลี่ยมแบบกราฟไฟท์ ถ่านกัมมันต์จากต้นกล้วยมีพื้นที่ผิวของวัสดุอยู่ในช่วง 517.67 ตารางเมตรต่อกรัม สำหรับถ่านกัมมันต์จากต้นกล้วยที่ ดัดแปรด้วยกำมะถัน, ออกซิเจน, กำมะถันและออกซิเจน และถ่านกัมมันต์ดัดแปรด้วยอิมิโน-ไทโอปิยูเรต มีพื้นที่ผิว 234.03, 453.74, 252.97 และ 22.96 ตารางเมตรต่อกรัม ตามลำดับ สำหรับการดูดซับ ถ่านกัมมันต์ต้นกล้วย (S-BSAC) ที่มีหมู่ฟังก์ชันที่มีกำมะถันเป็นตัวดูดซับมีความสามารถในการกำจัดตะกั่ว ได้ดี สภาวะที่เหมาะสมคือ 100 มิลลิตรต่อลิตร ของตะกั่ว(II) ไอออน, ในเวลา 2 ชั่วโมงที่ pH 6 และใช้ปริมาณสารดูดซับ 0.8 มิลลิกรัม การวิเคราะห์ทำโดยเครื่องอินดักทีฟพลัสเพลทาสมา โดยมีประสิทธิภาพในการกำจัดตะกั่วสูงถึง 99.78% ที่ความเข้มข้น 100 มิลลิกรัมต่อลิตร และสามารถใช้ซ้ำได้ถึง 3 รอบ

จุฬาลงกรณ์มหาวิทยาลัย  
CHULALONGKORN UNIVERSITY

สาขาวิชา เคมีสีเขียวและความยั่งยืน  
ปีการศึกษา 2565

ลายมือชื่อนิสิต .....  
ลายมือชื่อ อ.ที่ปรึกษาหลัก .....

# # 6478039623 : MAJOR GREEN CHEMISTRY AND SUSTAINABILITY

KEYWORD: ACTIVATED CARBON, BANANA STEM, ADSORPTION, LEAD

Imelda Octa Tampubolon : LEAD REMOVAL FROM WATER BY MODIFIED  
ACTIVATED CARBON PRODUCED FROM BANANA STEM. Advisor: Asst. Prof.  
Numpon Insin, Ph.D.

Banana stem-activated carbon (BSAC) and modified banana stem-activated carbon, containing sulfur, nitrogen, and oxygen-containing groups derived from banana stem, were prepared and studied for Pb(II) ion removal. The materials were characterized by scanning electron microscopy, X-Ray diffraction, surface area analysis, and Fourier transform infrared spectroscopy. SEM images showed that the materials are porous, and XRD confirmed that the structures are amorphous and resemble the graphitic hexagonal structure of carbon materials. Surface areas of these materials ranged from 517.67 m<sup>2</sup>/g for the bare banana stem activated carbon to 234.03, 453.74, 252.97, and 22.96 m<sup>2</sup>/g for sulfur, oxygen, sulfur and oxygen and imino-thiobiuret modified activated carbon. For the adsorption, sulfur-containing functional groups banana stem activated carbon (S-BSAC) was used as the adsorbent for lead removal. The optimized condition were 100 mg/L of lead(II) ions, 2 h of contact time, pH at 6, and 0.8 mg of adsorbent dosage. The analysis was done by inductively coupled plasma optical emission spectroscopy. The removal efficiency was as high as 99.78% for Pb(II) at 100 mg/L and could be used for 3 cycles.

Field of Study: Green Chemistry and  
Sustainability

Student's Signature .....

Academic Year: 2022

Advisor's Signature .....

## ACKNOWLEDGEMENTS

First of all, I would like to thank Jesus Christ, my God, Savior, Father, and Friend, for His love that never endures in my life.

I would like to thank Dr. Numpon Insin, my advisor, for his guidance, support, encouragement, and valuable advice through my research.

I also want to express my gratitude to Associate Professor Dr. Fuangfa Unob as the chairman committee and Dr. Samerkhae Jongthammanurak as the external examiner for all the valuable advice and comments throughout the proposal and thesis examination.

All members of Numpon Insin's lab, especially Miss Padtaraporn Chanchom, Mister Tirajate, and Mister Chonnavee Manipuntee, for their kind assistance.

Finally, I would like to offer my deepest gratitude to my parents, my sisters, and my brother for their love, prayer, and supports all the time.

## TABLE OF CONTENTS

	Page
ABSTRACT (THAI).....	iii
ABSTRACT (ENGLISH).....	iv
ACKNOWLEDGEMENTS.....	v
TABLE OF CONTENTS.....	vi
LIST OF TABLES.....	ix
LIST OF FIGURES.....	x
CHAPTER 1 INTRODUCTION.....	xii
1.1 Statement of the problem.....	xii
1.2 Objectives.....	2
1.3 Scopes of the thesis.....	2
1.3.1 Synthesis of BSAC.....	2
1.3.2 Modification of BSAC.....	3
1.3.3 Lead(II) ions adsorption experiments.....	3
CHAPTER 2.....	4
THEORY AND LITERATURE REVIEW.....	4
2.1 Contamination of lead in water reservoirs and its toxicity.....	4
2.2 Banana stem.....	4
2.3 Activated carbon.....	5
2.4 Preparation of activated carbon.....	6
2.4.1 Physical activation.....	6
2.4.2 Chemical activation.....	7

2.4.3 Surface modification of activated carbon .....	8
2.5 Adsorption .....	9
2.5.1 Physical adsorption.....	10
2.5.2 Chemical adsorption .....	10
2.5.3 Adsorption isotherm.....	11
2.6 Literature reviews .....	13
CHAPTER 3.....	17
EXPERIMENTS.....	17
3.1 Apparatus .....	17
3.2 Chemicals and reagents.....	18
3.2.1 Chemicals and reagents .....	18
3.3 Preparation of bare and modified-activated carbon.....	18
3.3.1 Synthesis of banana stem-activated carbon .....	18
3.3.2 Oxidation of banana stem-activated carbon.....	19
3.3.3 Sulfur-impregnation banana stem-activated carbon .....	19
3.3.4 Ammonia-impregnation banana stem-activated carbon .....	19
3.3.5 Modification of BSAC using 2-imino-4-thiobiuret .....	19
3.4 Characterization .....	21
3.5 Batch adsorption experiments .....	21
3.5.1 Effect of adsorption time .....	22
3.5.2 Effect of initial lead concentration .....	22
3.5.3 Effect of lead solution pH.....	22
3.5.4 Effect of co-existing cations.....	23
3.5.5 Reusability of the sorbent.....	23



CHAPTER 4.....	25
RESULTS AND DISCUSSION.....	25
4.1 Characterization of bare BSAC and modified BSAC .....	25
4.1.1 X-Ray diffraction .....	25
4.1.2 Surface area analysis.....	26
4.1.3 Surface morphology by scanning electron microscopy (SEM) .....	30
4.1.4 FTIR .....	33
4.2 Adsorption study .....	35
4.2.1 Study the adsorption of lead(II) at 100 mg/L of Pb <sup>2+</sup> solution .....	35
4.2.2 Effect of initial concentration.....	38
4.2.3 Adsorption isotherms .....	39
4.2.4 Effect of contact time.....	41
4.2.5 Adsorption kinetics .....	42
4.2.6 Effect of pH .....	44
4.2.7 Effect of adsorbent dosage.....	46
4.2.8 Effect of co-existing cations.....	47
4.2.9 Reusability of S-BSAC .....	48
CHAPTER 5.....	50
CONCLUSION .....	50
REFERENCES .....	52
VITA.....	61

## LIST OF TABLES

Table 2. 1 Surface modification of activated carbon for lead removal .....	13
Table 3. 1 List of Chemical .....	18
Table 4. 1 Surface area and pore diameter of the material .....	29
Table 4. 2 Elemental analysis of BSAC and modified BSAC .....	33
Table 4. 3 Adsorption efficiency and adsorption capacity of BSAC .....	36
and modified BSAC at 100 mg/L .....	36
Table 4. 4. The kinetic adsorption parameters .....	43
Table 5. 1 The adsorption behavior of S-BSAC and optimal conditions for the removal of Pb <sup>2+</sup> .....	50

## LIST OF FIGURES

Figure 2. 1 Lignocellulosic compound a) cellulose b) hemicellulose c) lignin .....	5
Figure 2. 2 Oxygen groups on activated carbon[33] .....	6
Figure 2. 3 Pore diagram of activated carbon .....	8
Figure 3. 1 Preparation and modification of BSAC .....	20
Figure 3. 2 Batch adsorption .....	24
Figure 4. 1 XRD pattern of a)BSAC, b)BSAC-COOH, c)S-BSAC, d)S-N(IT)-BSAC, e)S-N(Am)- BSAC .....	25
Figure 4. 2 Adsorption isotherm of a) BSAC .....	26
Figure 4. 3 Adsorption isotherm of b) BSAC-COOH c) S-N(am)-BSAC .....	27
Figure 4. 4 Adsorption isotherm of c) S-BSAC d) IT-BSAC .....	28
Figure 4. 5 SEM image and the elemental mapping of BSAC .....	30
Figure 4. 6 SEM image and the elemental mapping of BSAC-COOH .....	30
Figure 4. 7 SEM image and elemental mapping of S-BSAC .....	31
Figure 4. 8 SEM image and elemental analysis of IT-BSAC .....	31
Figure 4. 9 SEM image and elemental mapping of S-N(am)-BSAC .....	32
Figure 4. 10 FT-IR spectra of a) BSAC, b)BSAC-COOH .....	33
Figure 4. 11 FT-IR spectra of a) S-N-BSAC, b)S-BSAC, c)IT-BSAC .....	34
Figure 4. 12 The removal efficiency of a)BSAC, b)BSAC-COOH, c)S-BSAC, d)IT-BSAC and e) S-N(Am)-BSAC .....	36

Figure 4. 13 Effect of initial concentration on % removal efficiency of S-BSAC .....	38
Figure 4. 14 Effect of initial concentration on adsorption capacity of S-BSAC .....	38
Figure 4. 15 The Langmuir isotherm for Pb(II) sorption using S-BSAC .....	40
Figure 4. 16 The Freundlich isotherm for Pb(II) sorption using S-BSAC .....	40
Figure 4. 17 Effect of contact time on lead(II) ion removal efficiency of S-BSAC .....	41
Figure 4. 18 Effect of contact time on lead(II) removal adsorption capacity of S-BSAC. .....	42
Figure 4. 19 Adsorption kinetic data of lead(II) ion .....	44
Figure 4. 20 Effect of pH on lead(II) ion removal efficiency of S-BSAC .....	45
Figure 4. 21 Effect of pH on lead(II) ion adsorption capacity of S-BSAC .....	45
Figure 4. 22 Effect of adsorbent dosage on lead(II) ion removal efficiency and adsorption capacity of S-BSAC .....	47
Figure 4. 23 Selective adsorption of Pb(II) ion on S-BSAC .....	48
Figure 4. 24 Reusability study of S-BSAC in 3 cycles .....	49

# CHAPTER 1

## INTRODUCTION

### 1.1 Statement of the problem

Lead, known as the second most toxic metal, is primarily utilized in automobile and battery manufacturing, painting, mining, and metal plating [1]. The presence of lead(II) ions poses significant environmental concerns due to their persistence (non-biodegradable nature) and toxicity [2, 3]. Even a trace level of lead(II) ions can harm humans. Some reports have mentioned that adults absorb 5-15% of lead(II), and retained approximately 5% in their bodies. If the blood of living organisms contained 0.5-0.8 mg/mL of lead(II), it can lead to widespread health disorders, including dysfunction of brain, liver, kidney damage, pregnancy miscarriages in woman, hypertension lead shows toxicity in the liver, brain, nervous and reproductive systems [4, 5]. Children are more vulnerable to lead effects; their bodies absorb lead faster and higher than grown-ups, which is highly detrimental as they are developing [6].

Numerous treatment methods have been employed to remove lead(II) ions from water, including filtration [7], chemical precipitation [8], electrochemical treatment [9], liquid-liquid extraction [10], flocculation [11], ion exchange [12], adsorption, *etc.* Among the widely used methods, adsorption is preferred due to its cost-effectiveness, high efficiency, design flexibility, and various adsorbents' availability [13]. Adsorption is capable of removing heavy metal pollutants at lower than 100 mg L<sup>-1</sup> [14]. Moreover, the reversible nature of many adsorption processes, using suitable desorption processes, made the adsorption ideal for multiple uses. Showing some superior characteristics, which are large surface area, high porosity and well-developed structure, makes the activated carbon as a promising and widely used for adsorbent heavy metal [15]. Banana stem is a high potential precursor for producing activated carbon, as it is rich in lignin and cellulose contents, giving a high production yield, large surface area, and high fixed carbon content. This application gives a benefit in recycling the banana stem residues effectively.

Modifying the surface of activated carbon is done in purpose to increase its adsorption capacity towards Pb(II), the surface of activated carbon can be modified. Previous studies have demonstrated that the surface modification can be achieved by incorporating specific functional groups. Sulfur-containing and nitrogen-containing groups have been mainly utilized for Pb(II) ions removal [16]–[18]. These groups provide active sites to bond with Pb(II) through chelation to obtain higher adsorption. In this work, we chose activated carbon as a sorbent material due to its excellent properties. Doping the sulfur and nitrogen-containing groups onto the surface of activated carbon to enhance the lead(II) ion uptake and adsorption capacity.

## 1.2 Objectives

1. To synthesize banana stem-based activated carbon
2. To functionalize the activated carbon with amine-thiol functional groups to enhance lead removal capacity
3. To study the adsorption capacity and reusability of modified-banana stem-based activated carbon in removing lead(II) ions from water

## 1.3 Scopes of the thesis

This research consists of 3 parts: synthesized BSAC, modification of BSAC, and adsorption of lead(II) experiments in batch operation.

### 1.3.1 Synthesis of BSAC

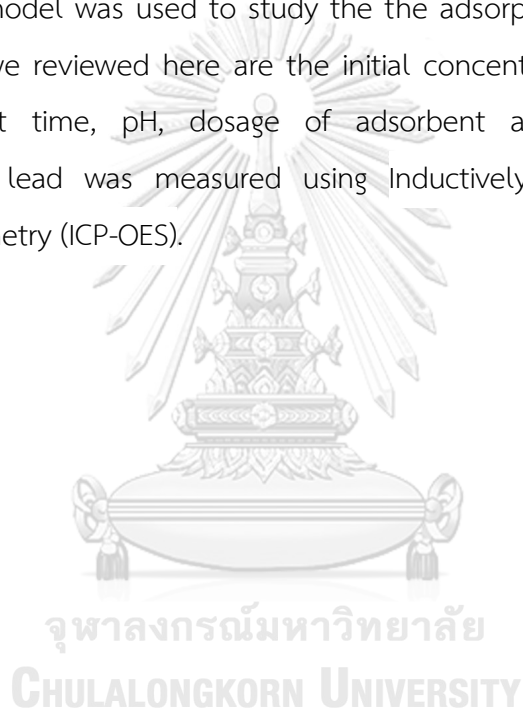
BSAC was synthesized from pyrolysis of banana stem impregnated with  $\text{H}_2\text{SO}_4$  with a ratio of  $\text{H}_2\text{SO}_4$  to the banana stem of 1:1 (w/w) at 600 °C under  $\text{N}_2$  atmospheric. The characterization was done using instruments such as scanning electron microscopy (SEM), surface area analyzer, Fourier-transform infrared spectroscopy (FTIR), and X-ray diffractometer (XRD).

### 1.3.2 Modification of BSAC

The modification of BSAC was conducted with 3 different methods, oxidation by using  $\text{HNO}_3$  20%, grafting by using 2-imino-4-thiobiuret, and modification by flowing  $\text{NH}_3$  gas. These modifications aimed to increase the number of some functional groups including sulfur, nitrogen, and oxygen-containing groups to improve the adsorption efficiency and capacity for lead(II) ion uptake from the water.

### 1.3.3 Lead(II) ions adsorption experiments

Batch operation model was used to study the the adsorption of lead(II) ions. Some parameters that we reviewed here are the initial concentration of lead(II) ions, the effect of contact time, pH, dosage of adsorbent and foreign cations. The concentration of lead was measured using Inductively coupled plasma-optical emission spectrometry (ICP-OES).



## CHAPTER 2

### THEORY AND LITERATURE REVIEW

#### 2.1 Contamination of lead in water reservoirs and its toxicity

Heavy metals occur naturally in the environment. However, anthropogenic or industrial activities can enrich them in a specific environment and even exceed the water quality or drinking water guidelines. Lead, a well-known heavy metals, is extensively utilized in industries such as mining, printing, painting, metallurgy, and electroplating [19]. Industrial waste from the abovementioned industries represents the primary source of lead(II) ions in water bodies. Lead is considered toxic if it is present in the environment, even at low concentrations. The accumulation of lead(II) ions in the body can cause severe and chronic diseases such as kidney damage, cancer, lung damage, and hypertension [20]. Lead(II) ions in drinking water mainly originate from the corrosion of household plumbing systems and natural deposits erosions.. Lead exposure has irreversible negative effects on children's cognitive function and development. A recent study highlighted that approximately 1 in 3 children worldwide (800 million children) currently have elevated blood lead levels which can significantly contribute to intellectual disabilities, decreased IQ, and reduced lifelong learning potential [21].

มหาวิทยาลัย  
CHULALONGKORN UNIVERSITY

#### 2.2 Banana stem

Banana is the world's acknowledged favourite fruit, first domesticated in Southeast Asia, then shifted to the most consumed and exported worldwide [22], [23]. Banana is widely ranked the fourth most-grown food crop worldwide. This fruit provides the essential nutrition source of potassium, vitamins A and C [23]. The high number of banana cultivation leads to a large amount of waste from the banana tree; mainly, the stem contributes 78% of the total waste [24]. After harvesting, the stems are left end ended in the field for months for natural degradation [25]. The



banana stem is rich in carbon content, composed of cellulose, hemicellulose, and lignin with the percentage of 43.3%, 20.6% and 27.8%, respectively [26].

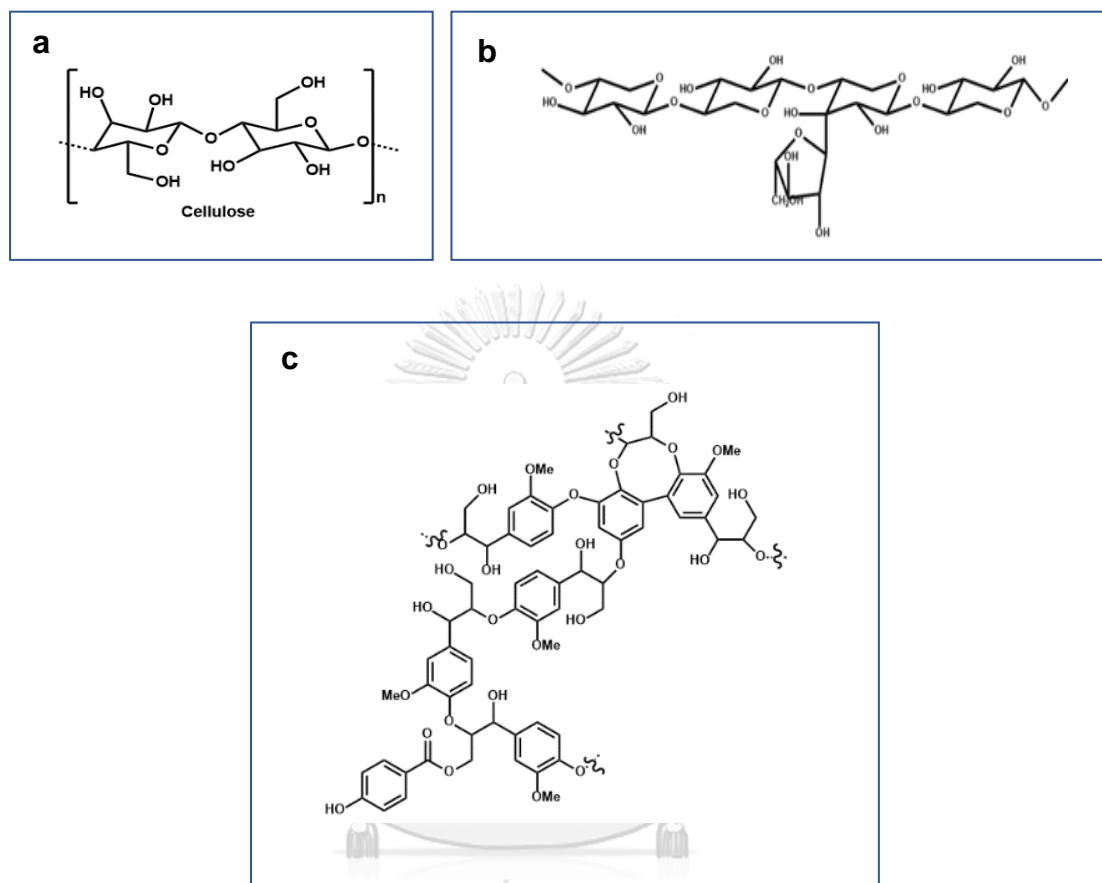


Figure 2. 1 Lignocellulosic compound a) cellulose b) hemicellulose c) lignin.

### 2.3 Activated carbon

Activated carbon is a porous carbonaceous material with excellent properties: well-developed pore structure, large specific surface area, and different surface functional groups. It finds extensive applications in wastewater treatment, air purification, and supercapacitor electrode material [27, 28]. The advantages of using activated carbon as an adsorbent are a simple process design, ease of implementation, resistance to corrosive and toxic environments, high adsorption potential for gas and liquid purification, and its ability to serve as supportive catalysts

[29]. Multiple raw materials can be used for producing activated carbon, including food crops, animals, petroleum byproducts, coal, and organic substances [30]–[32]. These materials are carbon-rich and undergo the carbonization process. The major functional groups are present in activated carbon including quinone, hydroxyl, carbonyl lactone and phenol contribute to the adsorption of water contaminants. Additionally oxygen, hydrogen, sulfur, and nitrogen may be present as functional groups or chemical atoms within the structure of activated carbon.

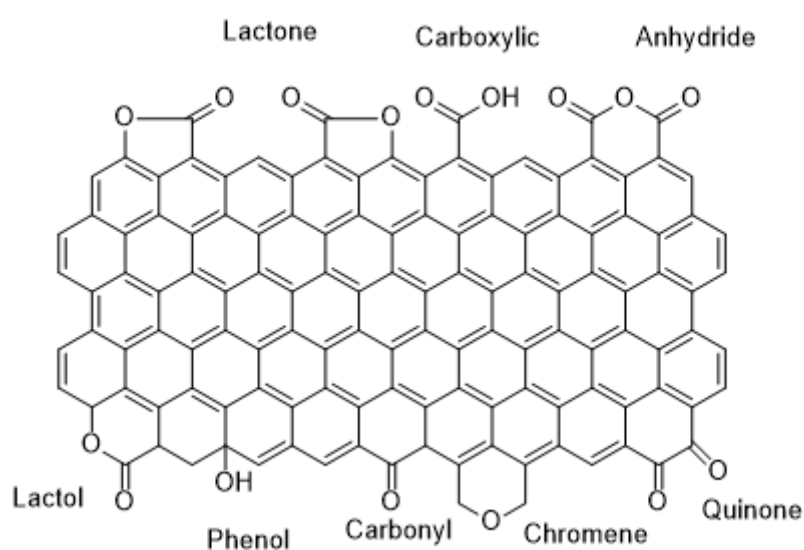


Figure 2. 2 Oxygen groups on activated carbon[33].

The adsorption behavior are influenced by various factors, including the functional groups present on the surface of activated carbon, precursor, activation processes, and thermal purification [34, 35].

## 2.4 Preparation of activated carbon

### 2.4.1 Physical activation

Physical activation is a two-step procedure comprising carbonization carbonization (pyrolysis) under a neutral atmosphere, followed by activation using oxidizing gases like carbon dioxide, and nitrogen or air mixtures. The temperature range for activation typically varies from 800–1100 °C [36]. This method is regarded as

cost-effective and environmentally friendly since it does not involve the use of chemicals [37, 38]. However, physical activation does have some drawbacks, including long activation time, relatively lower adsorption capacity of synthesized activated carbon, and high energy consumption [38].

#### 2.4.2 Chemical activation

Activated carbon can be prepared by wet oxidation, which involves activation in the presence of chemicals at high temperatures [38]. In the case of chemical activation, the process begins by saturating the raw material with highly dehydrated and oxidizing chemicals, called impregnation. Then, the suspension is dried, and the remaining mixture is then heated for a specified duration.

The temperature range for chemical activation can vary from 400 to 900 °C, depending on the activating material and the desired properties of the final product. During this process, cellulose undergoes degradation. The resulting mixture is subjected to repeated washing to obtain the activated carbon, and the final rinsing also aids in the recovery of active substances [39]. The chemical used in the activation agents act as dehydrating agents, influencing pyrolytic decomposition and inhibiting bitumen formation. This increases the carbon content of activated carbon and leads to changes in the thermal degradation of precursors, ultimately contributing to the development of the carbon's porous structure [40, 41]. These activating agents deeply penetrate the carbon structure, resulting in the formation of small pores in the activated carbon and an increase in surface area [41]. Unlike physical activation, in chemical activation, carbonization and activation occur simultaneously. This method is cost-effective as it requires lower activation temperatures, shorter processing times, and exhibits higher carbon efficiency. Additionally, chemically activated carbon tends to have a more porous structure compared to physically activated activation [42]. The chemical activation process involves the investigation of factors, such as the effect of chemical agent, impregnation ratio, carbonization temperature, and carbonization time [43, 44]. Commonly used chemicals as activators including potassium hydroxide (KOH), sodium hydroxide (NaOH), calcium chloride (CaCl<sub>2</sub>), and potassium carbonate (K<sub>2</sub>CO<sub>3</sub>),

acidic groups such as phosphoric acid ( $\text{H}_3\text{PO}_4$ ) and sulfuric acid ( $\text{H}_2\text{SO}_4$ ), intermediate metal salts such as  $\text{ZnCl}_2$  and other activating agents [45].

#### 2.4.3 Surface modification of activated carbon

Surface modification of activated carbon has been a subject of investigation for many years and has been shown to improve its performance. The adsorption capacity and removal efficiency are strongly influenced by factors such as the pore structure, surface area, and surface chemistry. The surface modification of material can enhance the adsorption capacity and removal efficiency by increasing the presence of active functional groups on the adsorbent surface that have a high affinity for metals. The most well-known methods for modification are impregnation, doping, and grafting. These modifications involve introducing functional groups, thereby altering the chemical properties, as well as affecting physical properties such as surface area and pore volume.

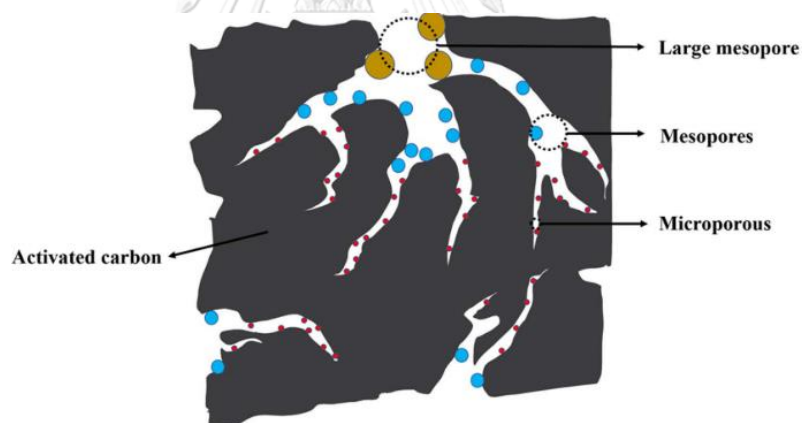


Figure 2. 3 Pore diagram of activated carbon.

The key factors in controlling the adsorption of heavy metals on activated carbon are:

a. Specific surface area

A large specific surface area is generally associated with a superior adsorption performance because it provides adsorption more space for adsorption to occur [46].

### b. Pore structure

Activated carbon possesses a porous structure, and its adsorption capacity for heavy metals is determined by its morphological structure, especially the pore size distribution [46]. Figure 2. 3 illustrates a schematic representation of the pores of the activated carbon. According to The IUPAC classifies, micropores have a radius of less than 2 nm, mesopores have a radius between 2 nm and 50 nm, and macropores have a radius greater than 50 nm [47]. The main sites of adsorption are micropores, while the mesopores aid in intra-particle diffusion, reducing the adsorption time. The macropores, also known as transport pores, serves as channels for the movement of heavy metals ions during adsorption. The metal ions enter the mesopores through the macropores, then migrate into the micropores, ultimately reaching the interior of activated carbon particles for adsorption.



### c. Functional groups

Functional groups present on activated carbon play an important role in adsorption process. The major functional groups attached to the activated carbon are oxygen, nitrogen, and sulfur, which act as the active sites for adsorption. The pollutants adhere to the surface of the activated carbon through various mechanism, including ion exchange, hydrogen bonding, electrostatic interaction, acid–base interaction, and complexation with the adsorbent [48]. The adsorption of heavy metals by activated carbon involves a combination of physical and chemical interaction, with the chemical functional groups on the surface of activated carbon playing a significant role alongside the morphology of activated carbon itself.

## 2.5 Adsorption

Adsorption refers to the process in which an adsorbate, which can be an ion or molecule present in liquid or gas, adheres to the surface of a solid adsorbent via mass transfer. This is a surface phenomenon, where only the surface of the

adsorption is involved, and the adsorbate does not penetrate the structure of the adsorbent. Unlike absorption, which involves the distribution of substance into bulk-phase materials, adsorption is a distinct mechanism. The reverse process, where molecules detach from the surface, is known as desorption.

### 2.5.1 Physical adsorption

Physical adsorption occurs ascribed to intermolecular forces, such as van der Waals, such as gas adsorption on activated carbon. It typically occurs at low temperatures, exhibits rapid adsorption rates, has a low heat of adsorption, and is non-selective. Since the effect of intermolecular attraction is weak, the structure of the adsorbate molecules hardly changes, leading to low adsorption energy and easy separation of the adsorbed substance. The process is reversible and the enthalpy of adsorption is typically around 20-40 kJ/mol.

### 2.5.2 Chemical adsorption

Chemical adsorption takes place through the formation of chemical bonds, usually covalent bonds, between the adsorbate and the surface of adsorbent. enthalpy change involved in chemical adsorption ranges from 40-400 kJ/mol. The process involves the formation and destruction of chemical bonds. It is irreversible and the chemical adsorption first increases and then decreases with the temperature increases.

### Hard/Soft Acid/Base (HSAB) theory

The principle of hard-soft acid-base (HSAB) was introduced by Pearson. HSAB is often employed to predict chemical reactivity, stability, and selectivity. Hard acids and bases are small and non-polarizable species, while soft acids and bases are large with more diffused electron distributions. The borderline acids are intermediate between hard and soft acids, possessing lower charge and larger size compared to soft acids. According to the HSAB principle, soft bases preferentially and strongly bind with soft acids, while hard bases exhibit a preference for hard acids [49]. Lead(II) ion

is categorized as a borderline acid, and making it challenging to find the bases that can form a stable complex.

### 2.5.3 Adsorption isotherm

Adsorption is characterized by a relationship that is independent of time representing the quantity of adsorbate attached to the adsorbent's surface in relation to the amount present in the surrounding environment. This relationship is expressed as if it is a gas or concentration for solutions. In wastewater treatment, the Langmuir, Freundlich, and BET models are commonly used as isotherm models to study the removal of heavy metal ions [50].

#### The Langmuir isotherm [51]

The Langmuir isotherm is an empirical model that proposes adsorption occurring at and equally definite localized sites on the adsorbent surface, forming a monolayer of adsorbed molecules [27]. According to this model, at a constant temperature, the adsorbate molecules undergo monolayer adsorption on a homogeneous adsorbent surface. The distribution of compounds between the two phases is controlled by the equilibrium constant when a monolayer of adsorbed material is formed over a uniform adsorbent surface. At equilibrium, the rates of adsorption and desorption are equal. The surface of the adsorbent has a specific number of sites where adsorbate molecules can be adsorbed. The Langmuir isotherm is mathematically described in Eq. 2.1.

$$q_e = \frac{q_m K_L C_e}{1 + C_e K_L} \quad (2.1);$$

where

$q_e$  = the amount of metal adsorbed per gram of the adsorbent of equilibrium (mg/g);

$C_e$  = the equilibrium concentration of adsorbate mg/L);

$q_m$  = maximum adsorption capacity (mg/g);

$K_L$  = Langmuir isotherm constant (L/mg)

The linear form of the Langmuir equation is shown in Eq. 2.2

$$\frac{C_e}{q_e} = \frac{1}{q_m K_L} + \frac{1}{q_m} C_e \quad (2.2)$$

### The Freundelich isotherm [27]

According to this model, adsorbate molecules undergo multilayer adsorption onto a heterogeneous adsorbent surface composed of several adsorption sites at a constant temperature. The Freundelich isotherm is shown in E.q 2.3

$$q_e = K_f C_e^{1/n} \quad (2.3);$$

where

$K_f$  = Freundelich isotherm constant (mg/g);

$n$  = adsorption intensity;

$C_e$  = the equilibrium concentration of adsorbate (mg/L);

$q_e$  = the amount of metal adsorbed per gram of the adsorbent at equilibrium (mg/g)

The values of  $n$  and  $1/n$  are temperature-dependent and provide information about the adsorption conditions such as adsorption intensity or surface heterogeneity. The linear representation of the Freundelich equation is given by Eq. 2.4.

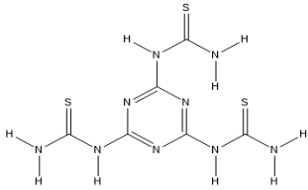
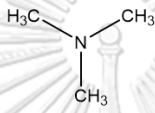
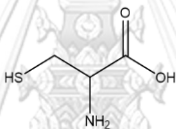
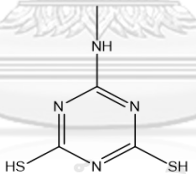
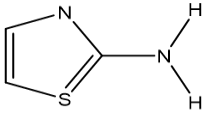
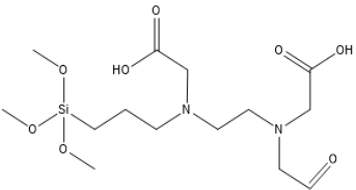
$$\ln q_e = \frac{1}{n} \ln C_e + \ln K_f \quad (2.4)$$

$K_f$  and  $1/n$  values can be determined from the linear plots of  $\log q_e$  versus  $\log C_e$ .



## 2.6 Literature reviews

Table 2. 1 Surface modification of activated carbon for lead removal

Adsorbent	Functional groups	Adsorption capacity (mg/g)	References
Triazine-based functionalized activated carbon		237.40	[16]
Functionalized corn husk derived Activated carbon		7.95	[52]
Activated carbon fibres modified by L-cysteine		179.53	[17]
Amine and thiol functionalized activated carbon		232.02	[53]
2-aminothiazole functionalized activated carbon		310.90	[54]
EDTA functionalized activated carbon		123.45	[55]
Fe-doped activated carbon	$\text{Fe}_2\text{O}_3$	124.30	[56]

Activated carbon is widely utilized for lead removal due to its favorable properties of large surface area, highly developed porosity, and high adsorption capacity. However, the bare activated carbon is not efficient enough for lead adsorption and needs to be modified with some functional groups to achieve higher adsorption capacity and efficiency. Table 2.1 summarizes the use of different functional groups for modifying activated carbon surfaces in lead removal from wastewater.

El-Wakil *et al.* [16] synthesized a novel chelating activated carbon (MT-MAC) by functionalizing activated carbon derived from water hyacinth (WH) with melamine thiourea (MT). The amidation was the main route for grafting between carboxyl groups of activated carbon and the amino groups of melamine thiourea (MT). Dicyclohexylcarbodiimide (DCC) was used as a coupling agent. The surface area of the material was 452.62 m<sup>2</sup>/g and its significant potential for adsorbing Pb<sup>2+</sup>, with an adsorption capacity of 237.4 mg/g.

Ismail *et al.* [52] synthesized the activated carbon from the corn husk waste, and then functionalized the surface of activated carbon with amine functional groups (the material label as AF-CHAC) by employing a series of chemical reactions involving epichlorohydrin, N-dimethylformamide, ethylenediamine. The BET surface area of the material was 442.70 m<sup>2</sup>/g, and it demonstrated a maximum adsorption capacity of 7.95 mg/g for Pb(II) ions.

For Zhu, L. *et al.* [17], the L-cysteine modified-activated carbon was synthesized by mixing sodium bisulfate (NaHSO<sub>4</sub>), activated carbon fibres (ACFs), and L-cysteine in the presence of hydrochloric acid solution and ethanol. Then, ACFs were added to the organic solvent, followed by Na<sub>2</sub>S as a reducing agent, to reduce the oxidized sulfhydryl group. The maximum adsorption capacity for Pb<sup>2+</sup> by L-cyst-ACF, determined using the Langmuir model, was 179.53 mg/g.

For Tang, N. *et al.* [53], thiol-functionalized AC (activated carbon) was prepared by dispersing the amine-AC into THF (tetrahydrofuran) followed by the addition of cyanuric chloride (CC) and N, N'- diisopropylethylamine (DIPEA). The product from the previous step was then mixed with sodium sulfide ( $\text{Na}_2\text{S}\cdot 9\text{H}_2\text{O}$ ) in water, then added addition of sodium carbonate. The Langmuir isotherm indicated the maximum adsorption capacity of 232.02 mg/g for  $\text{Pb}^{2+}$  at room temperature.

Waly, S. *et al.*[54] modified activated carbon derived from water hyacinth (HW) by chemical modification of activated carbon (AC) derived from water hyacinth (WH) via functionalization with 2-aminothiazole chelating agent (AT). The modification began with the oxidation of AC in nitric acid, named oxidized activated carbon (OAC). AT-MAC was prepared by dispersing OAC in an anhydrous DMF, followed by the addition of AT and DCC as coupling reagents. This material was utilized to effectively remove Pb(II) ions from polluted water. The AT-MAC adsorbent exhibited high sorption capacities for Pb(II) ions, with a value of 310.9 mg/g at pH 5.5 and a contact time of 60 min.

Lv, D. *et al.* [55], developed bamboo activated carbon (BAC) with ethylene diamine tetraacetic acid (EDTA) functionality by direct grafting in the presence of tetraethyl orthosilicate (TEOS) as a crosslinking agent. The values of surface area, mean pore diameter and pore volume of BAC@SiO<sub>2</sub>-EDTA were 69.92 m<sup>2</sup>/g, 4.83 nm, and 0.08 m<sup>3</sup>/g. The N<sub>2</sub> adsorption-desorption isotherm classified this material as Type IV isotherm (mesoporous material) according to the IUPAC classification of adsorption isotherms. The BAC@SiO<sub>2</sub>-EDTA material demonstrated a maximum adsorption capacity of 123.45 mg/g for Pb(II) ions, and the presence of EDTA promoted the formation of chemical complexes.

Chatla, A. *et al.* [56] employed wetness impregnation to dope the granular activated carbon (GAC) with Fe under various conditions. The conditions were varied, including the ratio of Fe to GAC (5% and 10%), water and ethanol served as solvent, and the nitrogen gas and air were used to study the effect of atmosphere of

pyrolysis. Then the Fe-doped materials were utilized for the adsorptive removal of lead(II) ions from the aqueous solution. The 5 wt% Fe-doped GAC impregnated in ethanol and calcined under nitrogen exhibited the highest surface area ( $715 \text{ m}^2 / \text{g}$ ) and pore volume. The Langmuir isotherm model yielded a maximum adsorption capacity of  $124.3 \text{ mg/g}$  for  $\text{Pb}^{2+}$  ions at pH 4.7 at room temperature.

Adly, M. *et al.* [57] reported high adsorption capacity for Hg(II) removal by grafting 2-imino-4-thiobiuret onto MIL-125 metal-organic framework. The Hg(II) adsorption capacity of this adsorbent was  $946 \text{ mg/g}$ . 2-imino-4-thiobiuret-functionalized activated carbon is a promising compound for functionalization of activated carbon. It has five active sites including two primary amines, two secondary amines and sulfur, that are ready to interact with Pb(II) through coordination bond, resulting in high adsorption capacity will be obtained. Moreover, 2-imino-4-thiobiuret modified activated carbon has not drawn much attention as an adsorbent for Pb(II).

The literature review showed that modifying by grafting amine and sulfur-containing groups or doping enhances adsorption capacity. This work used banana stem-activated carbon prepared by pyrolysis as an adsorbent. In order to obtain the high adsorption capacity, the BSAC was modified using sulfuric acid, ammonia gas, 2-imino-4-thiobiuret, and nitric acid and examined for lead(II) removal from water.

## CHAPTER 3

### EXPERIMENTS

The preparation of modified-banana stem activated carbon for lead(II) ions removal was divided into four parts:

#### Part 1: Preparation of banana stem-activated carbon

#### Part 2: Modification of banana-stem activated carbon

- Modification of BSAC with sulfur-containing group
- Modification of BSAC with nitrogen-containing group
- Modification of BSAC with oxygen-containing group

#### Part 3: Characterization of the modified-banana stem-activated carbon

#### Part 4: Adsorption study of lead

- Effect of time
- Effect of lead solution pH
- Effect of adsorbent dosage
- Effect of initial concentration
- Effect of foreign ions in Pb(II) removal operation
- Reusability of the materials

#### 3.1 Apparatus

- Fourier transform infrared spectroscopy (FT-IR), model: Impact 410 (Nicolet)
- X-ray diffraction (XRD), model: DMAX 2200/Ultima (Rigaku)
- Surface area analyzer, model: BELSORP-mini (BEL Japan)
- Scanning electron spectroscopy (SEM), model: JSM-54 10LV (JOEL)
- Inductively coupled plasma-Optical emission spectroscopy (ICP-OES), model: Thermo Scientific Icap 6000 SERIES

### 3.2 Chemicals and reagents

All chemicals were used without purification

#### 3.2.1 Chemicals and reagents

Table 3.1 List of chemicals

Chemicals	Suppliers
Sulfuric acid (conc.)	Merk
1000 g/ml of lead standard solution	Sigma-Aldrich
Nitric acid (conc.)	Merk
Nitrogen gas (Ultra High Purity grade)	Linde
Ammonia gas (Ultra High Purity grade)	Linde
2-immino-4-thiobiuret	Sigma-Aldrich
Sodium Hydroxide (99%)	Merk
Dimethylformamide (99%)	Merk
Hydrochloric acid (conc.)	Merk
N,N'-Dicyclohexylcarbodiimide	Sigma-Aldrich

### 3.3 Preparation of bare and modified-activated carbon

#### 3.3.1 Synthesis of banana stem-activated carbon

Approximately 10 kg of banana stem waste was initially obtained from a local banana farm in Salaya, Nakhon Pathom, Thailand. The collected banana stem biomass underwent washing and was subsequently dried under the sunlight for a duration of 5 days. To ensure constant mass, the drying process was continued using an oven. Then, the dried banana stem was finely ground into a powder using a grinding machine (Ji Gong Yi, JGB-800B) and sieved to achieve a size ranging between 30 – 70  $\mu\text{m}$  (200 mesh). The pretreated banana stem waste powder was mixed with  $\text{H}_2\text{SO}_4$  with a ratio (1:1 w/w). After allowing overnight impregnation, the resulting carbon slurry was washed with deionized water until a neutral pH solution was obtained. Finally, the slurry was dried at 100  $^\circ\text{C}$  for 24 h. Pyrolysis was conducted in

a muffle furnace at temperature of 600 °C for a duration of 30 min, while simultaneously flushing nitrogen gas at a flow rate of 3 °C/min. The resulting material, known as BSAC was then cooled to room temperature under nitrogen gas and stored in a vacuum desiccator for further use.

### 3.3.2 Oxidation of banana stem-activated carbon

1 g of BSAC was subjected to treatment with 30 mL of 20% HNO<sub>3</sub> under reflux at 90 °C for 3 h. The obtained material was washed with deionized water until a neutral pH was achieved and subsequently dried at 50 °C for 12 h. This material was labeled as BSAC-COOH [58].

### 3.3.3 Sulfur-impregnation banana stem-activated carbon

The pretreated banana stem waste powder was mixed with H<sub>2</sub>SO<sub>4</sub> with a ratio (1:1 w/w). After undergoing overnight impregnation, the slurry was calcinated in a muffle furnace at 600 °C for 30 min, while simultaneously being flushed with nitrogen gas at a flow rate of 3 °C/min. Then the material was washed with water until a neutral pH solution was obtained. The BSAC will then be cooled to room temperature under nitrogen gas and stored in a vacuum desiccator for further use. This material was labeled as S-BSAC.

### 3.3.4 Ammonia-impregnation banana stem-activated carbon

The oxidized BSAC was then calcinated at 600 °C in a muffle furnace for 60 min with ammonia gas being simultaneously flushed at a flow rate of 3 °C/min. After cooling down at room temperature, the gas was replaced with nitrogen. This material was labeled as S-N-BSAC.

### 3.3.5 Modification of BSAC using 2-imino-4-thiobiuret

0.20 g of BSAC-COOH was dispersed in anhydrous DMF (8 mL) through stirring at room temperature for 30 min. Then, 0.18 g of 2-imino-4-thiobiuret was added to the mixture, followed by 0.18 g of N,N'-Dicyclohexyl carbodiimide (DCC). Then, the

mixture was refluxed at 120 °C for 24 h, washed with DMF, then DI water, and finally dried at 60 °C for 24 h. This material was labeled as IT-BSAC [54].

The route of synthesis :

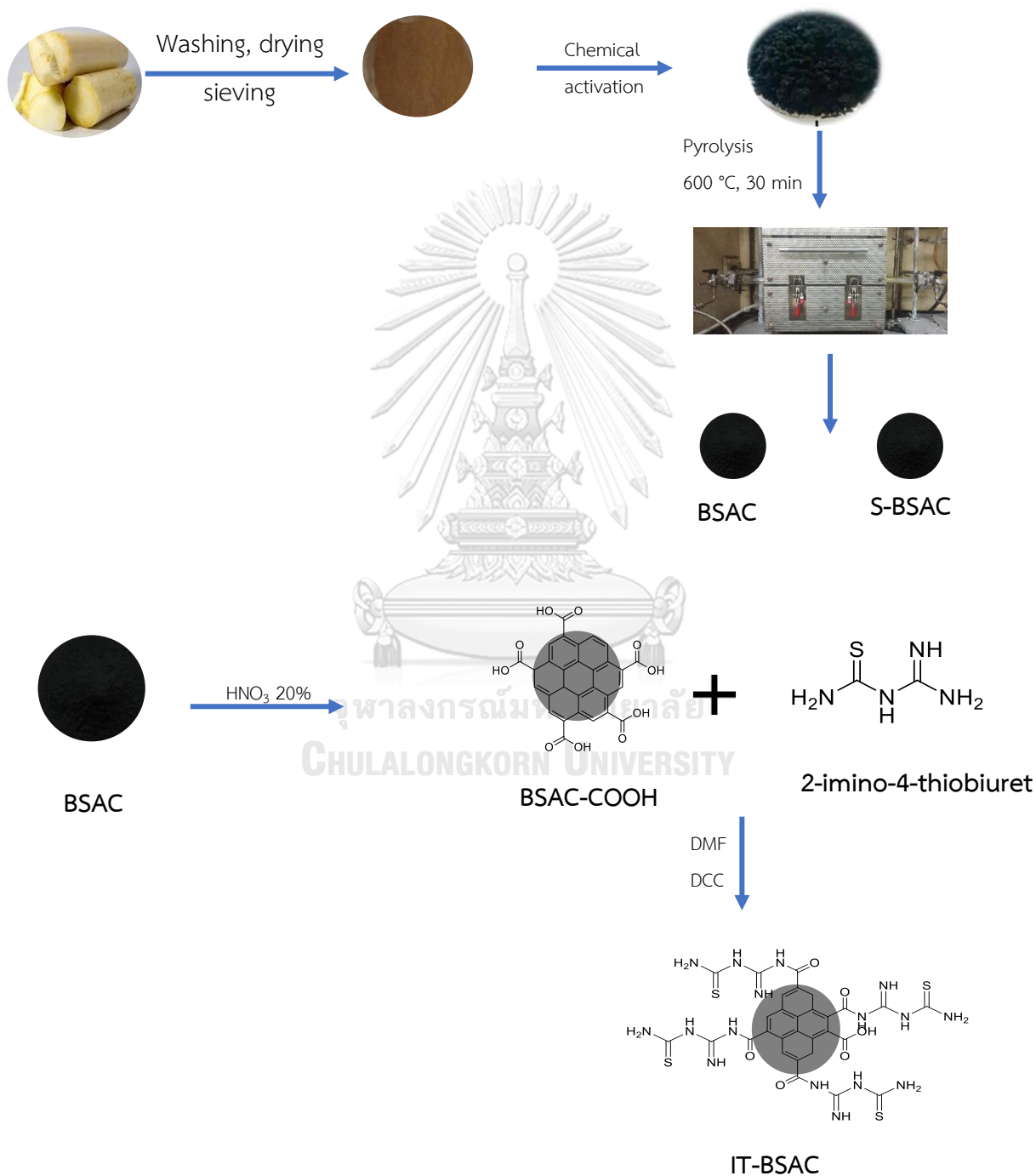


Figure 3. 1 Preparation and modification of BSAC.



### 3.4 Characterization

The synthesized materials underwent characterization using an X-Ray diffractometer. The XRD patterns were obtained at 2 theta ( $2\theta$ ) analysis angles in the range of 5 to 80 degrees, with a voltage at 40 kV, and an applied current of 30 mA. The diffractometer employed a fixed monochromator and a Cu  $K\alpha$  radiation source. The divergent, scattering, and receiving slits were set at 0.5°, 1°, and 0.3 mm, respectively.

To determine the functional groups, present on the surface of the materials, FT-IR measurements were conducted in transmission mode, covering wavelength ranges from 4000  $\text{cm}^{-1}$  to 500  $\text{cm}^{-1}$ . Prior to analysis, the samples were mixed with potassium bromide with a ratio of 1:100 and then pressed to make a thin layer.

SEM analysis was performed to characterize the surface morphology and conduct the elemental analysis of the materials. The small amount of samples were subjected to the carbon tape, and then analysis was done with the conditions: the voltage at 15 kV, WD in the range of 10 – 12.

The materials' specific surface area and mean pore diameter were determined using a surface area analyzer. Prior to analysis, the samples underwent pretreatment at 200 °C for 7 hours, followed by the adsorption-desorption of nitrogen gas at -196 °C.

### 3.5 Batch adsorption experiments

Batch adsorption experiments were used to investigate the adsorption of Pb(II) onto bare BSAC and modified BSAC. In each experiment, 0.02 g of the adsorbent was added into 25 mL of 10 to 100 mg/L Pb(II) solution at temperature of 30 °C. The pH of solutions was adjusted using  $\text{HNO}_3$  (0.01 M) or NaOH (0.01 M). The mixture was stirred for a duration of 2 h. Subsequently, the solid was separated from the solution through filtration. The initial and final concentrations of the metal were determined using Inductively coupled plasma optical emission spectroscopy (ICP-OES).

The removal efficiency, R (%), was determined using Eq. (3.1), where  $C_0$  and  $C_e$  are initial and final concentrations ( $\text{mg L}^{-1}$ ), respectively.

$$\text{Sorption}\% = \frac{C_0 - C_e}{C_0} \times 100\% \quad (3.1)$$

The adsorption capacity was calculated using the following Eq. (3.2):

$$q_e = \frac{C_0 - C_e}{m} \times V \quad (3.2)$$

Where  $C_0$  and  $C_e$  ( $\text{mg/L}$ ) are initial and equilibrium concentrations of Pb(II), respectively;  $V$  ( $\text{cm}^3$ ) is the volume of solution, and  $m$  is the mass of sorbent (g) used.

### 3.5.1 Effect of adsorption time

25 mL lead(II) solution was in contact with 0.02 g of adsorbent in a series range of time in 5, 15, 30, 60, 90, 120, and 150 min at 30 °C. The initial concentration of lead(II) ion was 100 mg/L. The pH was fixed at 6.

### 3.5.2 Effect of initial lead concentration

The initial lead concentrations were studied at different concentrations, which are 10, 25, 50, 100, 150, 200, and 250 mg/L. The pH was fixed at 6 and the temperature at 30 °C. This experiment's contact time is when the maximum adsorption was obtained.

### 3.5.3 Effect of lead solution pH

The effect of solution pH on lead adsorption ( $\text{Pb}^{2+}$  initial concentration of 100 mg/L) was studied in the initial pH range of 3, 4, 5, and 6. The pH of the initial solution of  $\text{Pb}^{2+}$  was adjusted to the desired values using 0.01 M  $\text{HNO}_3$  or 0.01 M NaOH.

#### 3.5.4 Effect of co-existing cations

Wastewater is prepared by adding various metal ions into lead solutions. In each experiment, 0.02 g sorbents were added into a 25 mL mixture containing Zn(II)/Pb(II), Mg(II)/Pb(II), and Cu(II)/Pb(II) with concentration 100 mg/L.  $Zn^{2+}$  is the borderline acid,  $Mg^{2+}$  is the hard acid naturally present in water, and  $Cu^{2+}$  is a soft acid. Study the series of metals to see the selectivity of adsorbent is important. The mixture is stirred for two h at room temperature. The sorbents are filtered, and the final Zn(II), Mg(II), Cu(II), and Pb(II) concentrations are determined using Inductively Coupled Plasma Optical Emission spectroscopy (ICP-OES).

#### 3.5.5 Reusability of the sorbent

In a batch operation, 0.02 g of S-BSAC was investigated after the sorbent was used in lead adsorption. The pH of the solution, the concentration of Pb(II), and the duration of the process were set to optimize the adsorption capacity. The amount of adsorbent was stirred with Pb(II) solution and then separated from the mixture through centrifugation. The spent adsorbent was treated by suspending it in 50 mL of  $1.0 \text{ mol L}^{-1}$  HCl for 2 h. After centrifugal separation, the adsorbent was thoroughly washed with deionized water to completely remove any remaining chloride ions. The treated adsorbent was reused for adsorbing Pb(II) again. This procedure was repeated 3 times using the same method and the levels of Pb in the supernatant after centrifugation were measured.



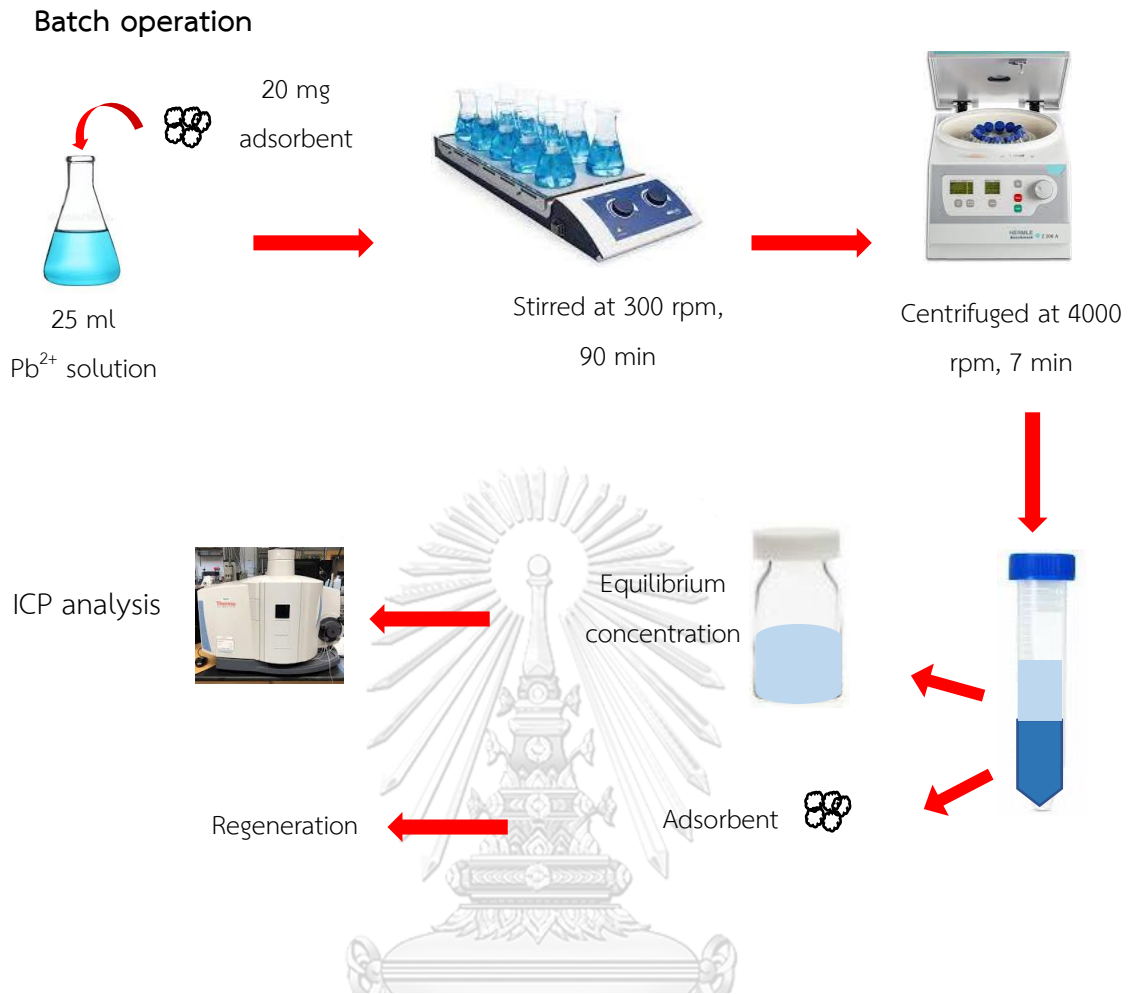


Figure 3. 2 Batch adsorption.

## CHAPTER 4

### RESULTS AND DISCUSSION

#### 4.1 Characterization of bare BSAC and modified BSAC

##### 4.1.1 X-Ray diffraction

BSAC and modified BSAC materials were characterized by using an X-Ray diffractometer. This analysis aims to see the amorphousness of all the carbon materials. The powdered X-ray diffractogram has been carried out for BSAC and modified BSAC in the  $2\theta$  range of  $5^\circ$  to  $80^\circ$  to identify the nature of the materials.

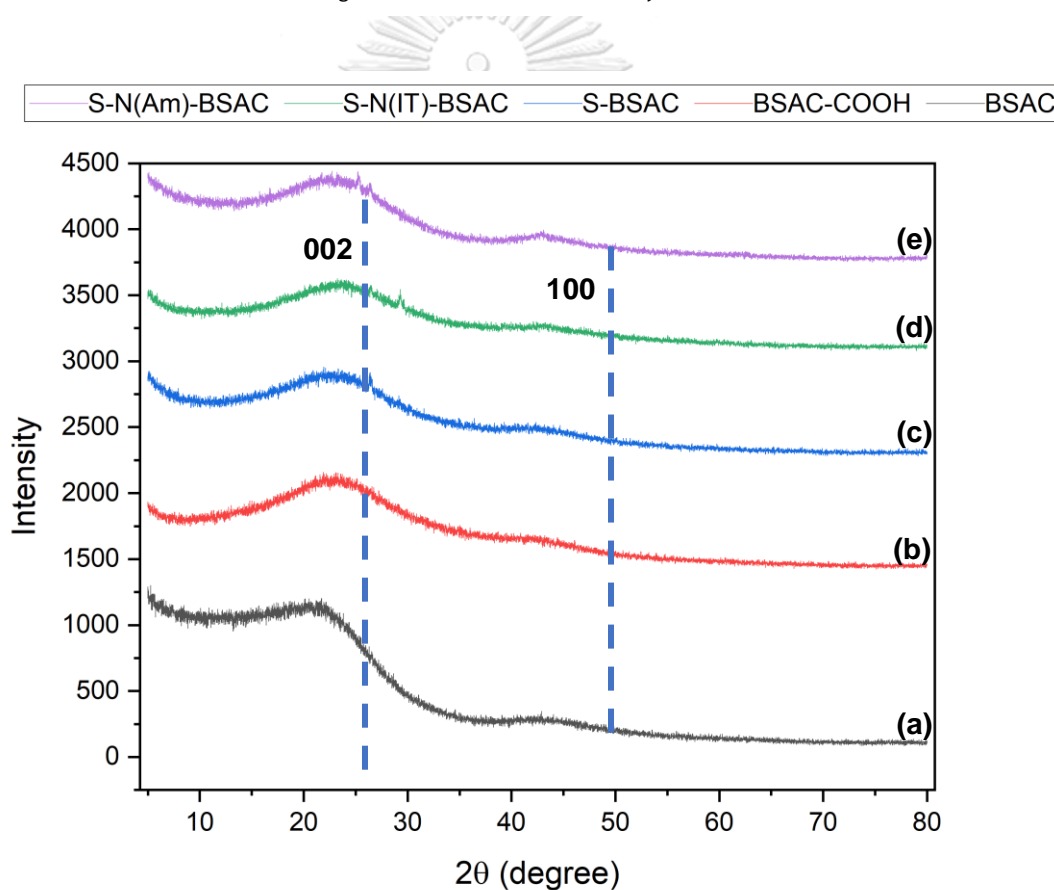


Figure 4.1 XRD pattern of a) BSAC, b) BSAC-COOH, c) S-BSAC, d) S-N(IT)-BSAC, e) S-N(Am)-BSAC.

The prominent broad peak at  $2\theta$  value of  $23^\circ$  and a faint broad hump peak at  $43.1^\circ$  corresponded to the reflection planes (0 0 2) and (1 0 0) respectively, suggesting the presence of a hexagonal and disordered structure and coherent, parallel stacked graphene-like sheets in both BSAC and modified-BSAC [28]. This finding indicates a similarity to the graphitic hexagonal structure commonly found carbon-based materials, as confirmed by the JCPDS 00-056-0159. The graph (Figure 4.1) shows the amorphous nature of the adsorbents as a significant portion of the materials constitutes a carbon base. The pyrolysis at  $600^\circ\text{C}$  and modification of BSAC did not create the crystal structure.

#### 4.1.2 Surface area analysis

The surface area of both bare and modified activated carbon was determined using nitrogen adsorption-desorption. The data obtained from the adsorption-desorption isotherm were utilized to calculate the specific surface area (SSA) by BET method ( $S_{\text{BET}}$ ), as well as to determine the mean pore diameter of materials.

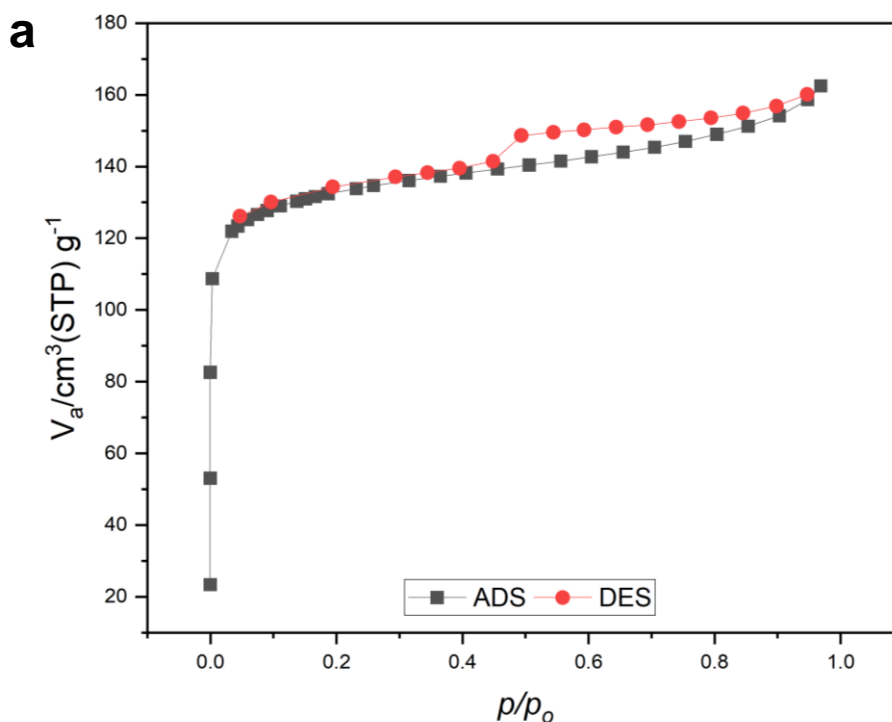


Figure 4.2 Adsorption isotherm of a) BSAC.

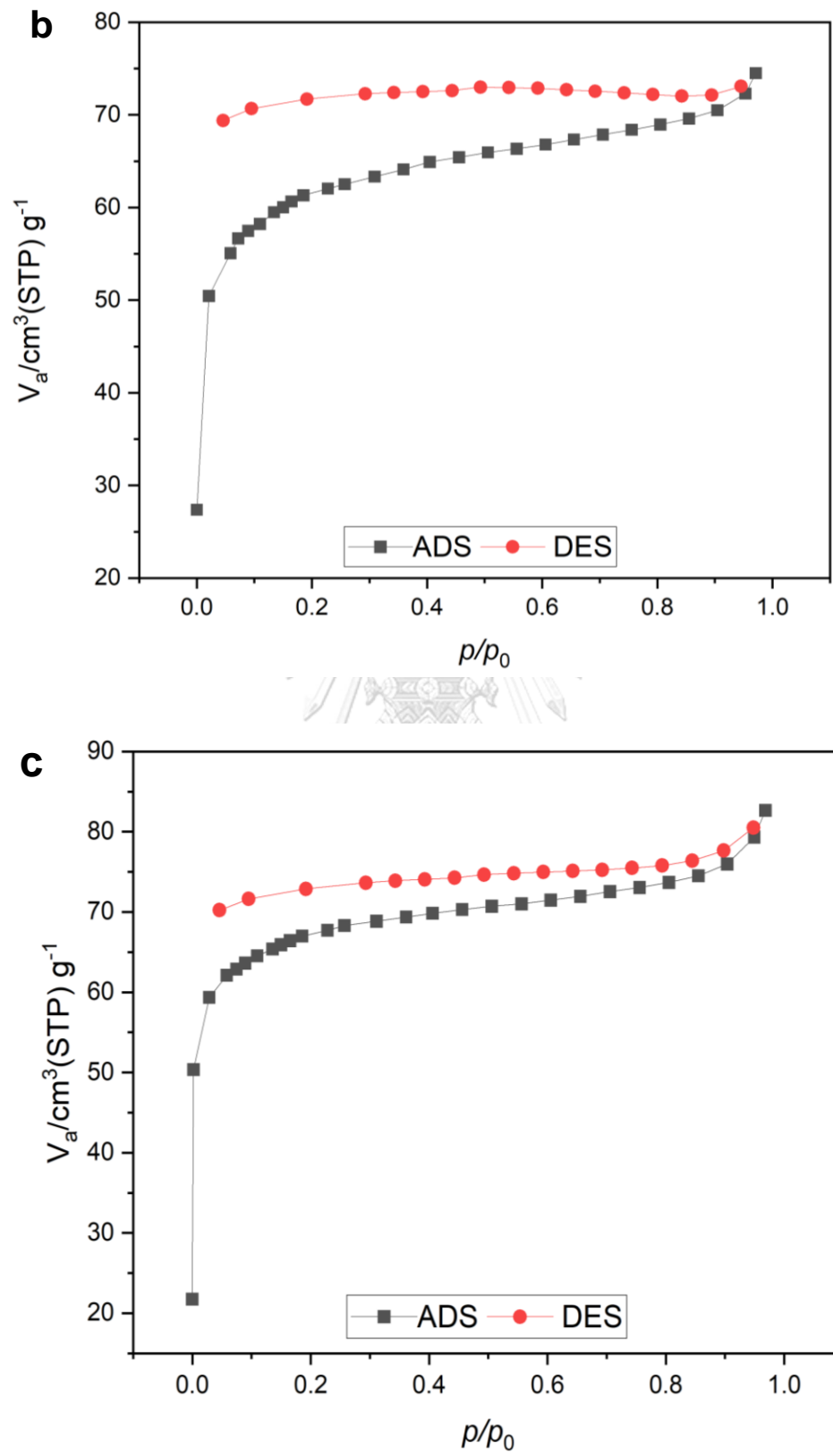


Figure 4.3 Adsorption isotherm of b) BSAC-COOH c) S-N(am)-BSAC.

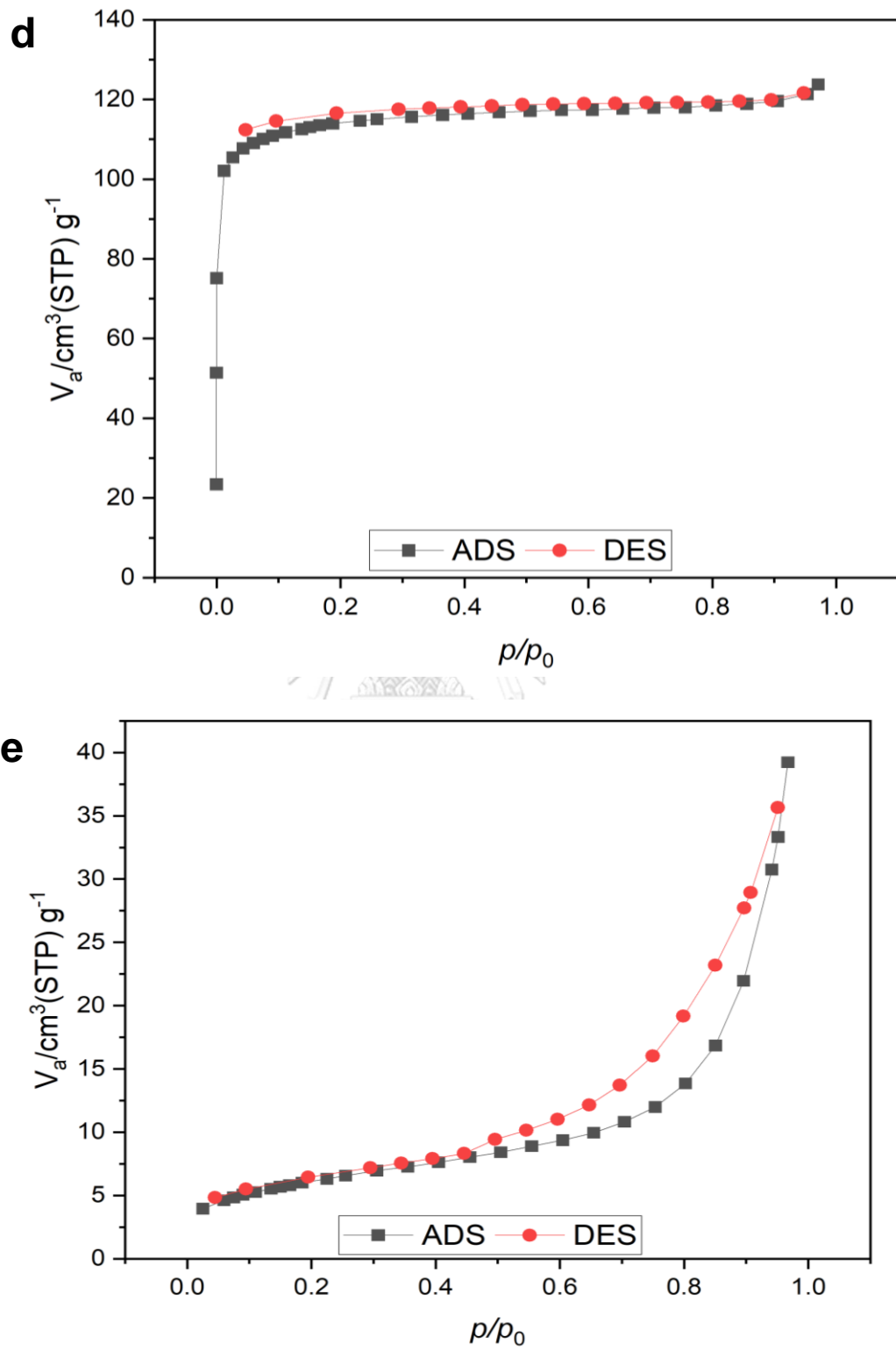


Figure 4. 4 Adsorption isotherm of d) S-BSAC e) IT-BSAC.



Table 4.1 Surface area and pore diameter of the materials

**a**

Materials	Surface area (m <sup>2</sup> /g)	Mean pore diameter (nm)	Total pore volume (cm <sup>3</sup> /g)
BSAC	517.61	1.94	0.25
BSAC-COOH	234.03	1.97	0.12
S-BSAC	453.74	1.69	0.19
S-N-BSAC	252.97	2.02	0.13
IT-BSAC	22.96	8.87	0.06

BSAC (Figure 4. 2) and S-BSAC (Figure 4. 3 c) exhibited Type 1 (microporous) but still had some mesoporous due to the narrow hysteresis loop H1. The hysteresis loop occurred at  $P/P_0 > 0.4$ . The absorbance of Type 1 isotherm increases rapidly at low relative pressure ( $0 < P/P_0 < 0.2$ ) and steadily increases at moderate pressure before attaining a constant value at  $P/P_0 > 0.95$ , revealing that the adsorbent has a micropore and mesopore. The surface area and mean pore diameter of BSAC and S-BSAC are 517.61 m<sup>2</sup>/g, 234.03 m<sup>2</sup>/g, 1.94 nm, and 1.69 nm, respectively. BSAC-COOH and S-N(am)-BSAC displayed a Type 1 adsorption isotherm, characterized by an open loop, the loop that remains unclosed, even at low relative pressure ( $P/P_0 < 0.1$ ). This open loop could be attributed to the expansion of the adsorbent during the adsorption process or the presence of both physical and chemical adsorption mechanism to some extent [59]. Another possibility is that there may be limited development of micropore volume, or the pores are too small to accommodate the nitrogen molecules. Due to this phenomenon, it is suggested that the analysis may be conducted by using CO<sub>2</sub> gas at 0 °C. The CO<sub>2</sub> molecule is smaller than nitrogen, and the measurement temperature is high, so it will be a good way to accelerate diffusion. The surface area and mean pore diameter of BSAC-COOH and S-N(am)-BSAC are 234.03 m<sup>2</sup>/g, 252.97 m<sup>2</sup>/g, 1.97 nm, and 2.02 nm, respectively.

Modification using 2-imino-4-thiobiuret resulted in a large mean pore diameter. Nitrogen adsorption capacity IT-BSAC is less than 40 cm<sup>3</sup>.g<sup>-1</sup>, indicating that

the amount of nitrogen adsorbed was reduced after oxidation and modification. The isotherm demonstrated as Type IV (mesoporous).

#### 4.1.3 Surface morphology by scanning electron microscopy (SEM)

The SEM images reveal the surface morphology of all the adsorbents. SEM images of the adsorbents are shown in Figures 4. 5 - 4. 9.

The morphology of BSAC and modified BSAC was rough, with broken edges arranged in a parallel-layered graphene-like sheet. The main composition of all materials is carbon, with a percentage of more than 70%, which confirms that the banana stem is rich in carbon content. The elemental mapping confirms that the BSAC only contains carbon and oxygen (Table 4.2). The nature of this material is highly hydrophobic compared to the other materials because the composition of carbon is more than 90%. The particle size distribution ranged from 30 – 70 microns, as the banana stem was sieved in 200 mesh sieves while activated carbon was prepared. The surface porosity was enhanced upon pyrolysis because of the volatile matter released.

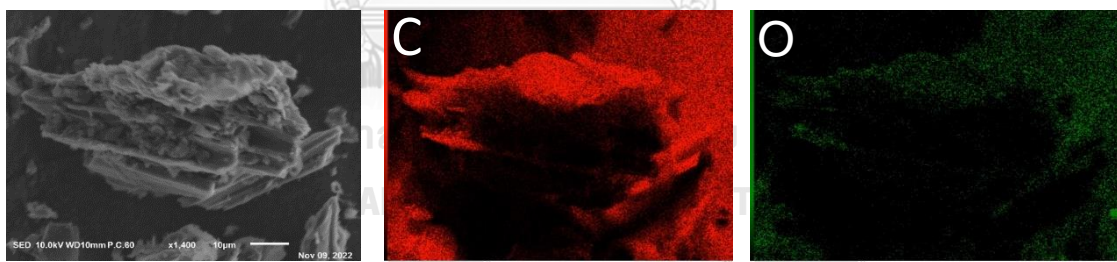


Figure 4. 5 SEM image and the elemental mapping of BSAC.

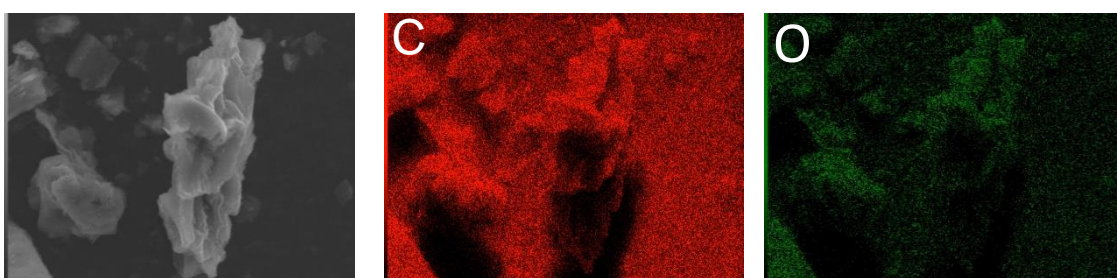


Figure 4. 6 SEM image and the elemental mapping of BSAC-COOH.

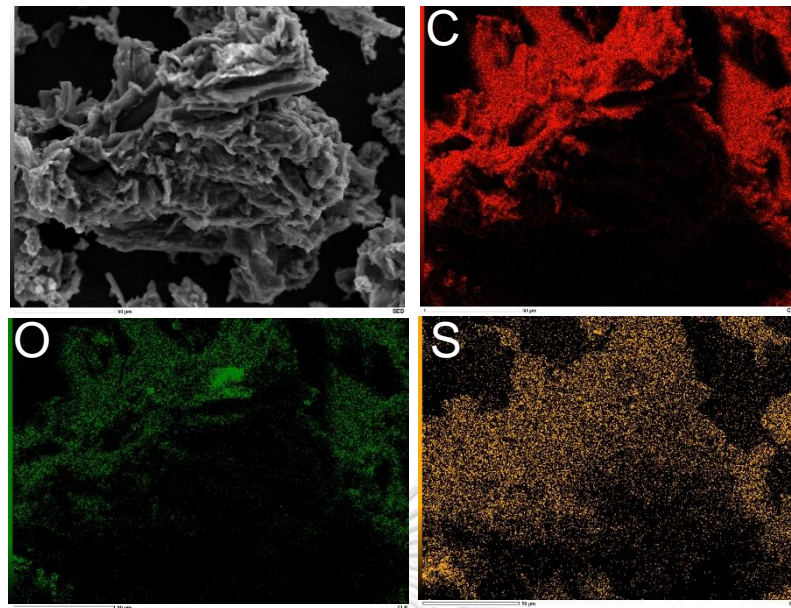


Figure 4. 7 SEM image and elemental mapping of S-BSAC.

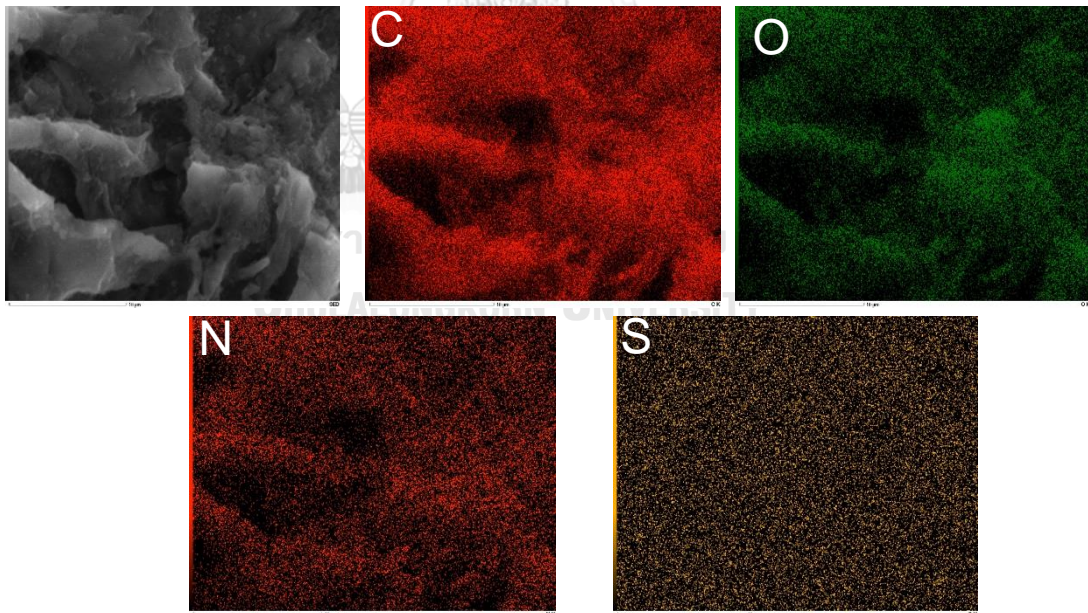


Figure 4. 8 SEM image and elemental analysis of IT-BSAC.

The roughness was increased when the modification occurred, and the wrinkled surface was observed due to the exfoliation and etching on the surface of

BSAC in the presence of nitric acid as a strong oxidizer (Figure 4. 6), promoting more oxygen groups attached to the surface of activated carbon. The nitrogen-functional group was introduced (Table 4.2) onto the activated carbon surface when ammonia gas and 2-imino-4-thiobiuret. After further modification with 2-imino-4-thiobiuret (Figure 4. 8) and ammonia gas (Figure 4. 9), the wrinkled surface of the activated carbon was observed due to the grafting of 2-imino-4-thiobiuret ligand into the surface and edges of BSAC and the presence of nitrogen from the ammonia gas on the surface of activated carbon.

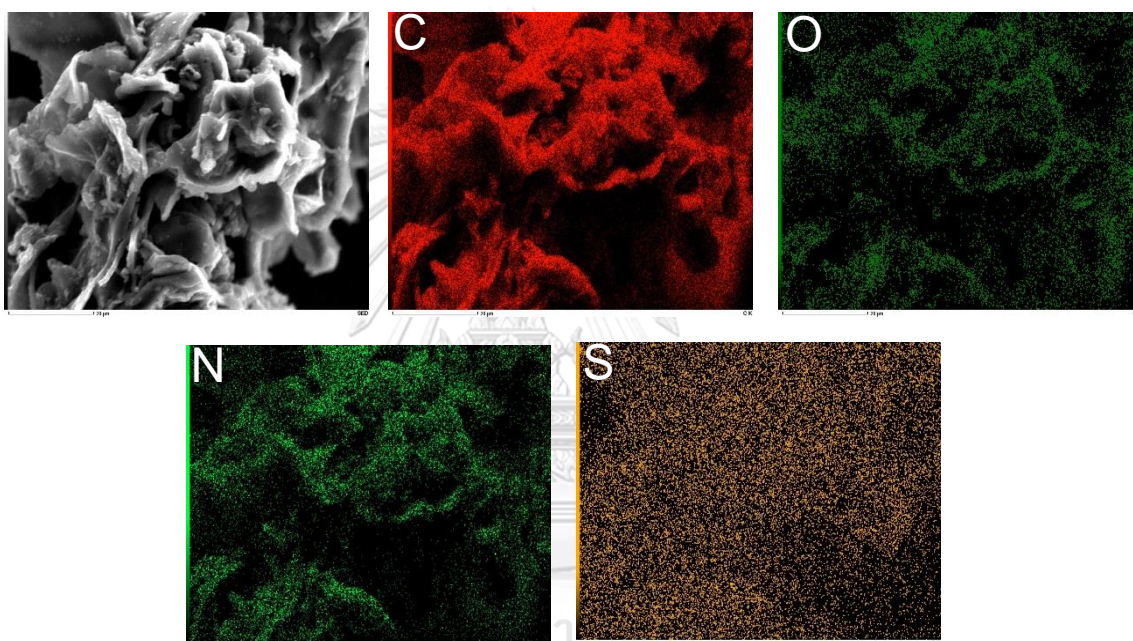


Figure 4. 9 SEM image and elemental mapping of S-N(am)-BSAC.

Table 4.2 Elemental analysis of BSAC and modified BSAC

Materials	Elemental analysis (Wt%)			
	C	O	N	S
BSAC	90.38	9.62	-	-
BSAC-COOH	74.87	25.13	-	-
S-BSAC	73.21	23.66	-	3.13
S-N-BSAC	82.66	12.72	2.71	1.88
IT-BSAC	70.79	26.14	1.46	1.61

#### 4.1.4 FTIR

FT-IR determined the qualitative characteristic of surface functional groups of BSAC and modified BSAC. The features of BSAC are displayed in Figure 4. 10. The FTIR spectra showed a weak band between  $3400 - 3200 \text{ cm}^{-1}$  for the O-H bond stretching. A signal at  $1583 \text{ cm}^{-1}$  corresponds to C=C in the aromatic ring [60]. After the oxidation by nitric acid, there is a significant increase in the intensity of the bands at  $3400 - 3200 \text{ cm}^{-1}$  and  $1724 \text{ cm}^{-1}$ , indicating that more carboxylic groups have been created on the surface of BSAC.  $1610 \text{ cm}^{-1}$  corresponds to C-O stretching vibrations of carboxylic groups, ketones, aldehydes, or lactones observed [61].

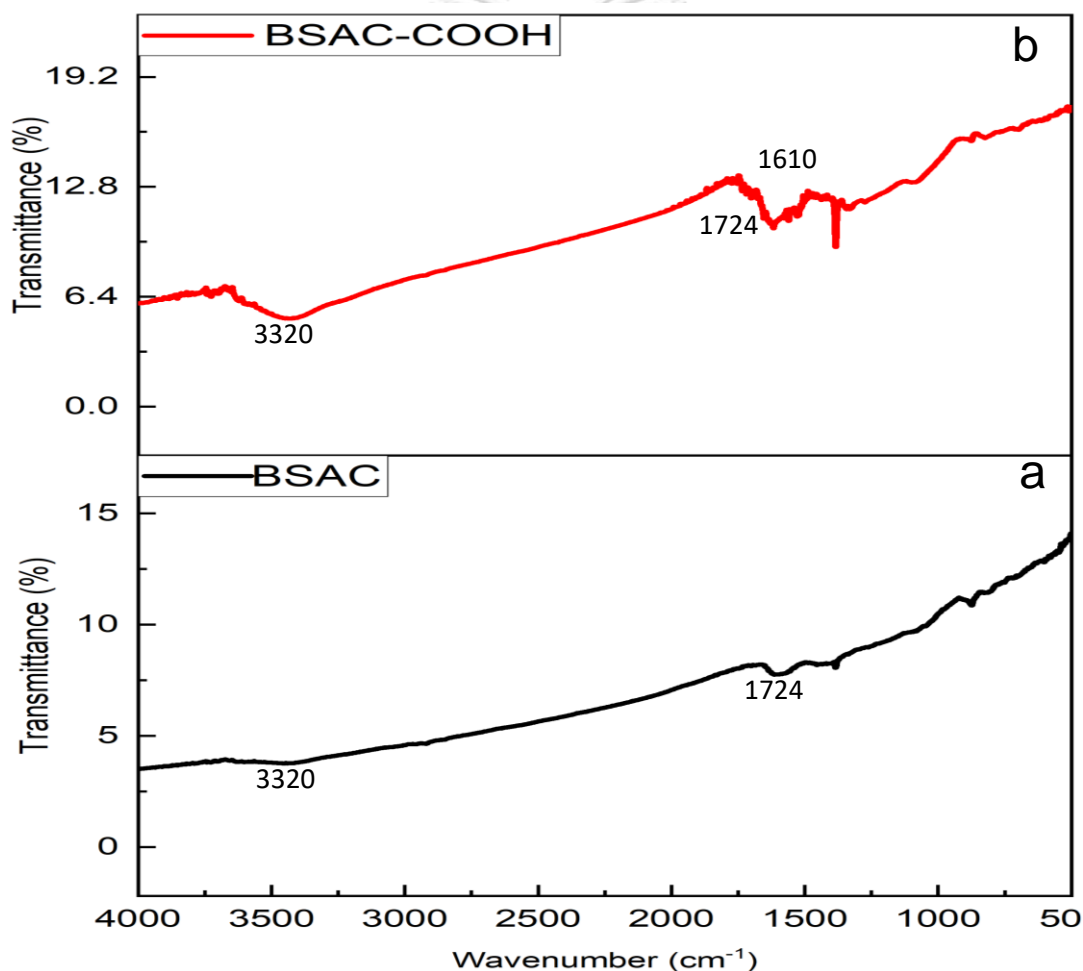


Figure 4. 10 FT-IR spectra of a) BSAC, b) BSAC-COOH.

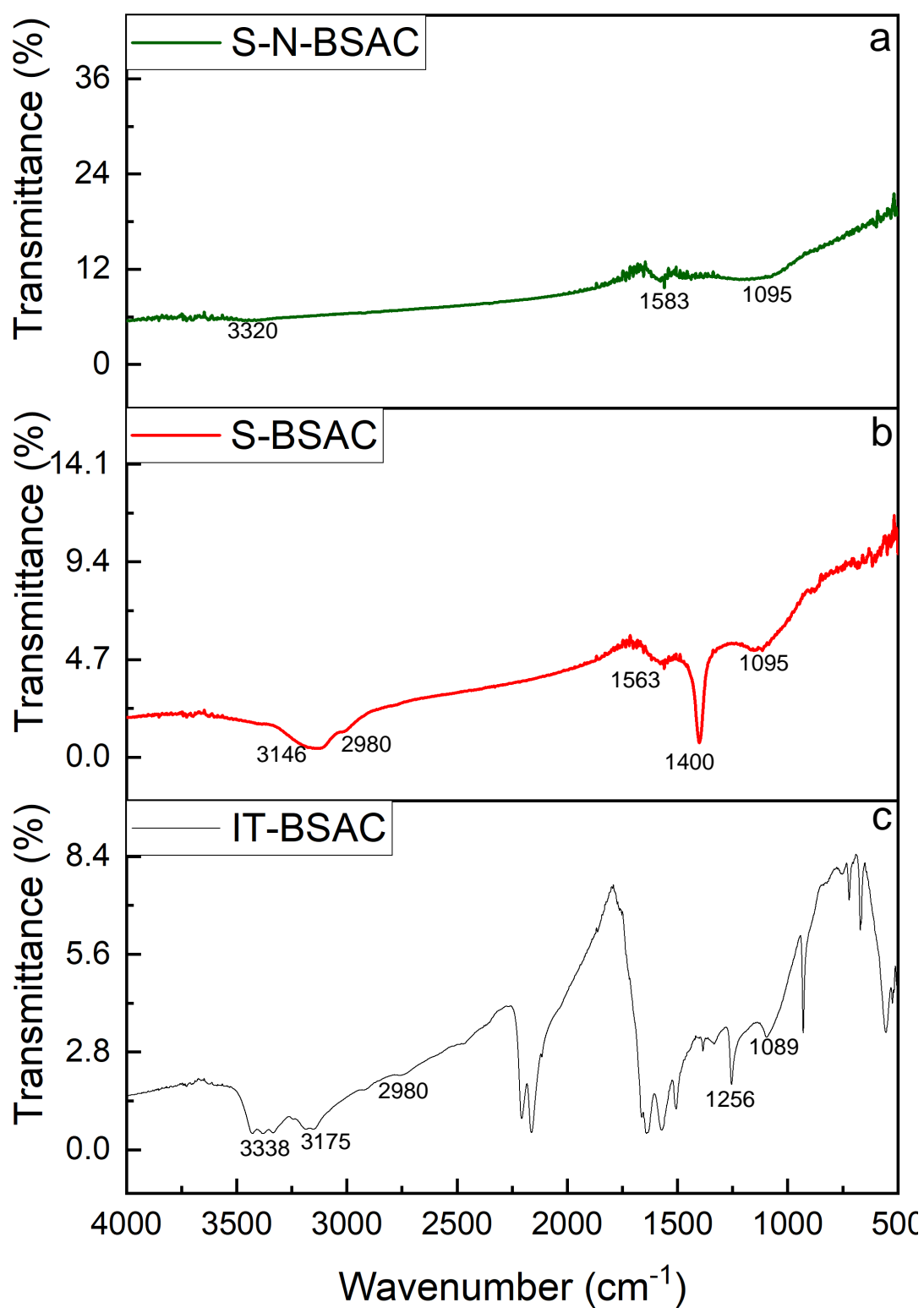


Figure 4. 11 FT-IR spectra of a) S-N-BSAC, b) S-BSAC, c) IT-BSAC.

The surface modification of BSAC into S-N(Am)-BSAC by flowing ammonia gas does not significantly change the surface of activated carbon. The amount of oxygen-containing groups such as hydroxyl reduced as the sample was carbonized for second time at 600 °C for 60 min. The nitrogen was introduced but hardly seen from the FTIR spectra; it could be overlapped with the O-H stretching at wavenumber 3200  $\text{cm}^{-1}$ .

Sulfur-containing groups were introduced onto the surface of activated carbon by impregnation. Prior to the calcination, the sample was dehydrated by using sulfuric acid. The FTIR spectra showed a new peak at 1400  $\text{cm}^{-1}$  corresponding to S=O stretching of sulfoxide, an adsorption peak at 3146  $\text{cm}^{-1}$  corresponding to O-H stretching of the hydroxyl group. Stretching vibrations in alkyl C-H groups can be seen in the adsorption bands 2980  $\text{cm}^{-1}$ .

The functionalization with 2-imino-4-thiobiuret created new bands at 3175  $\text{cm}^{-1}$  and 3338  $\text{cm}^{-1}$  in the BSAC-IT spectra. Those peaks are attributed to the C-N stretching vibration of the amide group and the N-H stretching vibration of the  $\text{NH}_2$  [62]. Bands at 1089 and 1256  $\text{cm}^{-1}$  are characteristic of -C=S vibrations [63].

## 4.2 Adsorption study

### 4.2.1 Study the adsorption of lead(II) at 100 mg/L of $\text{Pb}^{2+}$ solution

By batch operation, the adsorbents were studied for removing lead(II) ions in 25 mL  $\text{Pb}(\text{II})$  solutions at room temperature. The pH of the solution was adjusted to 6.

To test the adsorption capacity of each batch. 20 mg of each material were introduced to 100 mg/L  $\text{Pb}(\text{II})$  solution for 90 min. The removal efficiency and adsorption capacity of all materials are presented in Table 4.3.

Table 4. 3 Adsorption efficiency and adsorption capacity of BSAC and modified BSAC at 100 mg/L

Materials	% Removal (%)	Adsorption capacity (mg/g)
BSAC	23.52	29.40
BSAC-COOH	39.95	49.94
S-BSAC	99.82	124.78
IT-BSAC	36.03	45.04
S-N(Am)-BSAC	69.82	87.28

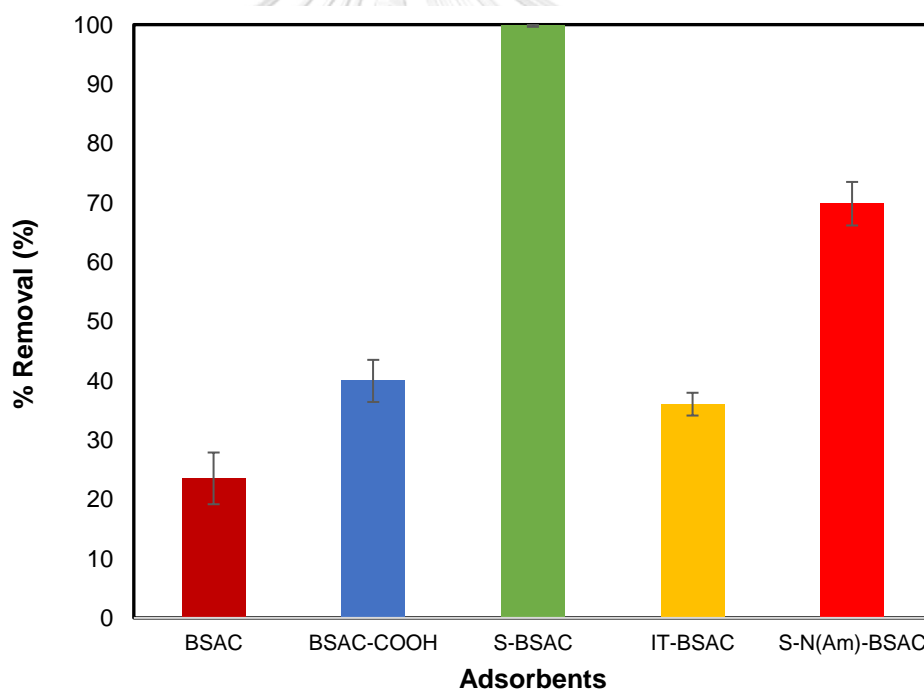


Figure 4. 12 The removal efficiency of a) BSAC, b) BSAC-COOH, c) S-BSAC  
d) IT-BSAC and e) S-N(Am)-BSAC



This study showed that the only sorbent that worked well at the high concentration was S-BSAC, and it indicated that the S-BSAC performed as a promising sorbent for lead(II) ions removal from solutions. For BSAC, as mentioned above, ascribed to the high carbon content and the small number of oxygen-containing groups, this material became hydrophobic, resulting in low adsorption efficiency and capacity. Hydrophobicity caused this material could not be dispersed well in water, so the chance to bind by physical or chemical interaction to  $Pb^{2+}$  was limited.

Adsorption efficiency and adsorption of BSAC-COOH increased slightly because the oxidation introduced some carboxyl groups to the surface of BSAC, given the higher number of carboxylic on the surface of BSAC-COOH. However, oxidation caused the micropores were broken and collapse due to the harsh condition, as nitric acid is a strong oxidation agent and led to a low surface area, affecting the efficiency and adsorption capacity. The electrostatic interaction seems to be between  $Pb^{2+}$  and oxygen-containing groups. The modification with 2-imino-4-thiobiret, caused the destruction even more significant to the pores. The pores became mesopores with a diameter of 8 nm. This sorbent showed great adsorption efficiency at low concentrations but became less effective at high concentrations due to less micropores and low surface area.

S-BSAC and N-BSAC performed well at high concentrations due to nitrogen and sulfur. S-BSAC is the best material in this work. It's main characteristics are high surface area ( $453.74 \text{ m}^2/\text{g}$ ), rich in micropores and sulfur-containing groups (including thiophene, sulfone and sulfide, caused by the pyrolysis). On batch operation, it showed the adsorption capacity reached 124.78. The presence of sulfur-containing groups contributes in removing  $Pb^{2+}$ , and the chelating and electrostatic interaction is the primary interaction in this work.

From all the results mentioned above, later in this work, the subsequent stages of this study focused on using S-BSAC to investigate the effects of initial concentration, adsorbent dosage, time, and pH. Furthermore, the influence of interfering cations in Pb(II) solutions and the reusability of S-BSAC were also examined.

#### 4.2.2 Effect of initial concentration

The initial concentration of lead solution was tested at various initial concentration of  $Pb^{2+}$  ranging from 10, 25, 50, 100, 150, 200, and 250 mg/L. The experiments were conducted at room temperature and at pH 6.

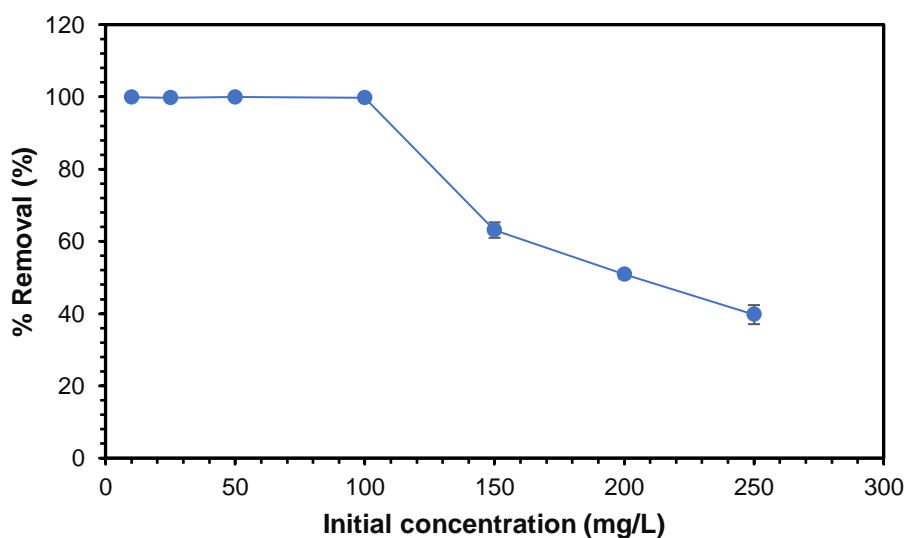


Figure 4. 13 Effect of initial concentration on % removal efficiency of S-BSAC.

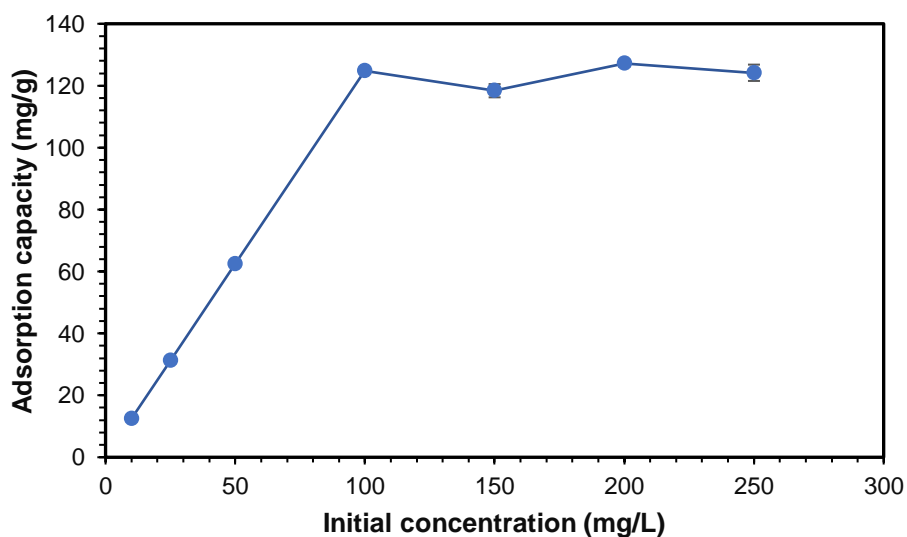


Figure 4. 14 Effect of initial concentration on adsorption capacity of S-BSAC.

Figures 4. 13 and 4. 14 demonstrated the high adsorption capacity and efficiency of BSAC. The removal efficiency of S-BSAC remained, reaching 99.8%, for initial concentration ranging from 10 – 100 mg/L, about 99.8%, but decreased as the initial concentration rose due to the saturation of sulfur-containing groups' binding sites in the adsorbent.

#### 4.2.3 Adsorption isotherms

The lead(II) adsorption data was used to study the sorption isotherms of the sorbent material. The adsorption behavior of the S-BSAC is investigated on the adsorption capacity at different initial concentrations using the Langmuir isotherm model and the Freundlich isotherm model. The Langmuir isotherm model was based on the assumption of the monolayer adsorption mechanism and homogenous chemisorption on the adsorbent surface. In contrast, the Freundlich isotherm model relates to the assumption of the irregular multilayer adsorption on the adsorbent surface. The adsorption isotherms were studied at the initial Pb(II) concentration of 100 – 250 mg/L, pH 5, adsorbent dosage 0.02 g, Pb(II) solution 25 mL, and contact time 90 min.

Langmuir isotherm model:

$$\frac{C_e}{q_e} = \frac{1}{q_m K_L} + \frac{1}{q_m} C_e \quad (4.1)$$

Freundlich isotherm model:

$$\ln q_e = \frac{1}{n} \ln C_e + \ln K_f \quad (4.2);$$

where

$q_e$ : the adsorption capacity at equilibrium (mg/g),

$C_e$ : the equilibrium concentration (mg/L),

$q_m$ : the maximum adsorption capacity (mg/g),

$K$ : the Langmuir isotherm constant

$K_f$ : the Freundlich isotherm constant

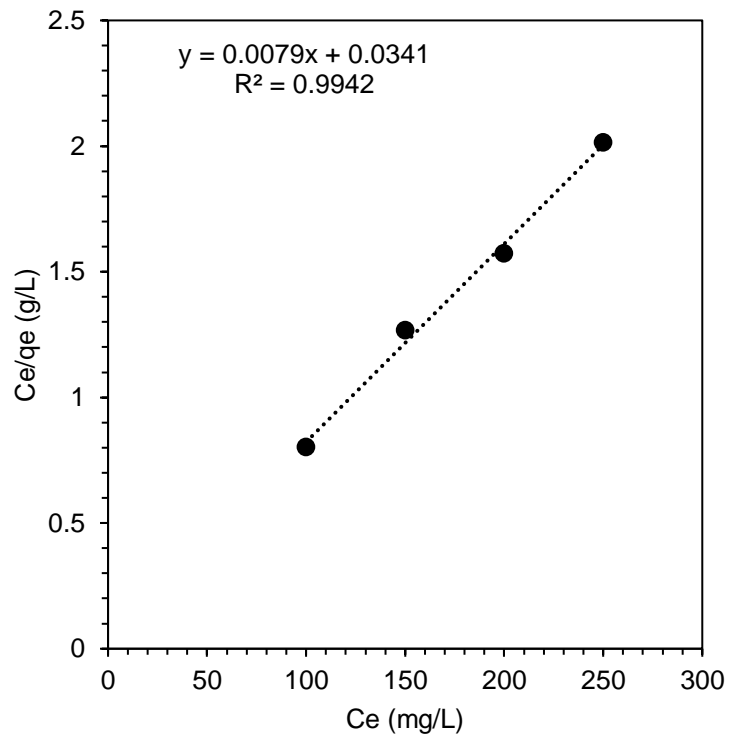


Figure 4. 15 The Langmuir isotherm for Pb(II) sorption using S-BSAC.

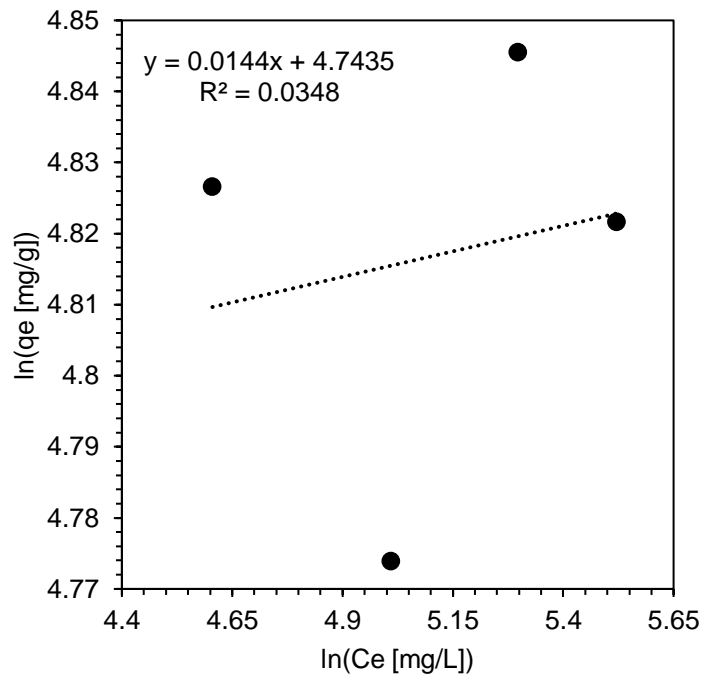


Figure 4. 16 The Freundlich isotherm for Pb(II) sorption using S-BSAC.

Adsorption isotherm  $Pb^{2+}$  S-BSAC was suitable to be described by the Langmuir isotherm model, as the correlation coefficients value of the Langmuir isotherm of S-BSAC ( $R^2 > 0.99$ ) is better than the correlation coefficient value of the Freundlich isotherm ( $R^2 > 0.034$ ) as depicted in Figures 4.15 and 4. 16. The maximum capacity of lead(II) sorption by S-BSAC was determined to be 126.85 mg/g, which closely aligned with the maximum observed adsorption capacity in the experiment.

#### 4.2.4 Effect of contact time

The effect of contact time at various time intervals (5 to 150 min) of S-BSAC (0.8 g/L) for lead removal with a concentration of 100 mg/L at pH 6 is presented in Figures 4. 17 and 4. 18.

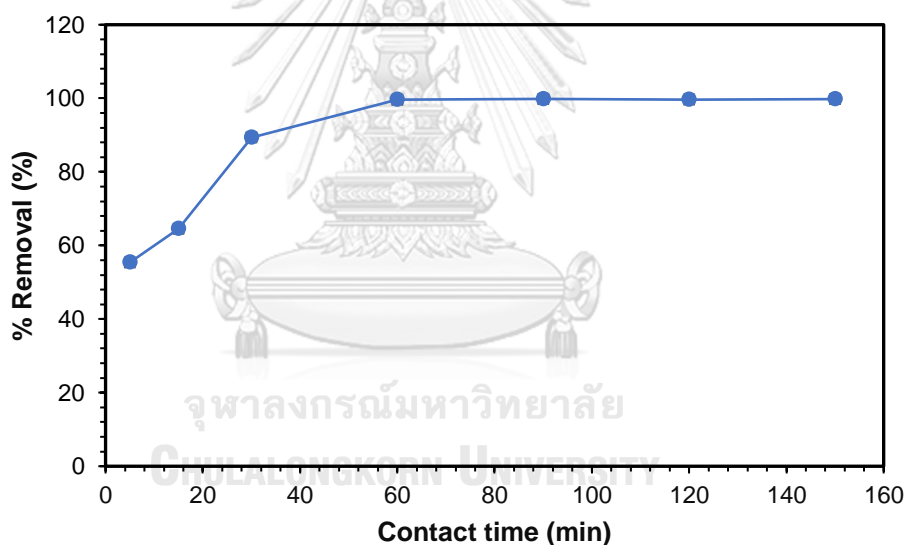


Figure 4. 17 Effect of contact time on lead(II) ion removal efficiency of S-BSAC.

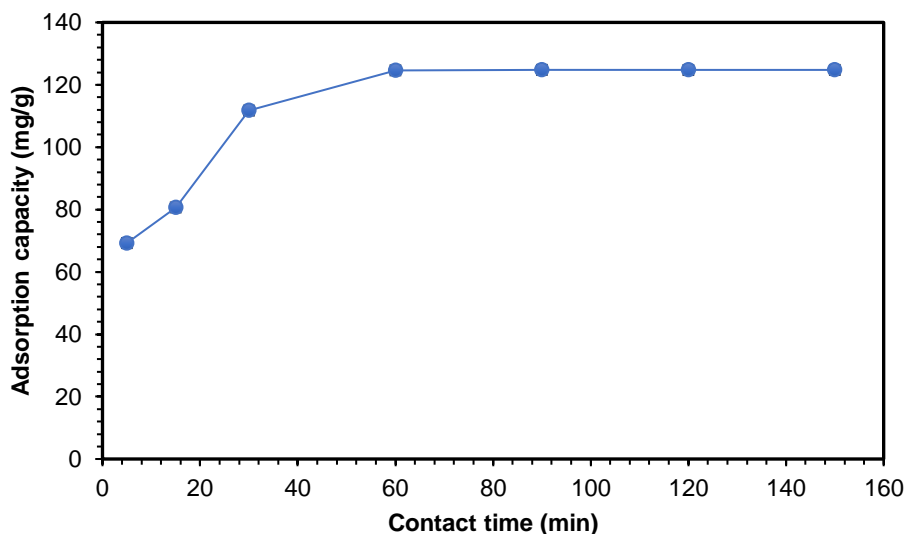


Figure 4. 18 Effect of contact time on lead(II) removal adsorption capacity of S-BSAC.

The lead removal efficiency and adsorption capacity exhibited an increasing trend over time until the equilibrium was achieved between the absorbed lead on S-BSAC and the remaining solution within 90 min. The aforementioned figures illustrate that the lead adsorption gradually increases from 5 min to 60 min and then reaches the plateau towards at the end of the experiment. This suggests that the adsorption process is initially fast, then gradually slow down and is constant after the optimum period at 90 minutes. The reason is the availability of the active sites at the initial period time. Once the active sites become saturated, equilibrium was reached at the 90 min mark, as the active sites became saturated. The removal efficiency at equilibrium was 99.82%, and the adsorption capacity reached 124.78 mg/g.

#### 4.2.5 Adsorption kinetics

Understanding the adsorption kinetics is crucial for assessing the adsorbent's performance, as it provides insights into the underlying chemical (reaction) and physical interaction. Adsorption kinetic is used to elucidate the mechanisms and reaction rate of the adsorption process. The relationship between the amount of adsorption and contact time is exhibited in Figure 4. 19. The fast rate of adsorption could be observed in the first 30 minutes, and after that, it became slower. It can be

understood that the remaining adsorption site is decreased caused by the occupation of lead(II) ions. The equilibrium was achieved within 90 minutes. Two kinetic models were employed to study the adsorption process: the non-linear pseudo-first-order kinetic model and the non-linear pseudo-second-order kinetic model. Non-linear models are generally preferred as they maintained error distribution characteristics, unlike linear techniques. These models are expressed in equations (4.3) and (4.4), respectively:

$$q_t = q_e(1 - e^{-k_1 t}) \quad (4.3)$$

$$q_t = \frac{k_2 q_e^2 t}{1 + k_2 t q_e} \quad (4.4);$$

where :

$q_t$ : is the adsorption capacity (mg/g) at time t

$q_e$ : is the adsorption capacity (mg/g) at the equilibrium

t: is the contact time (min)

$k_1$ : is the first order rate constant ( $\text{min}^{-1}$ )

$k_2$ : is the second order rate constant (g/mg min).

Non-linear plots of  $q_t$  versus t and the results of kinetic adsorption are presented in Figure 4. 19 and in Table 4.4 respectively.

Table 4.4 The kinetic adsorption parameters

Pseudo-first-order model			Pseudo-second order model		
$k_1$	$q_e$	$R^2$	$k_2$	$q_e$	$R^2$
0.1052	122.19	0.79	0.0013	130.97	0.91

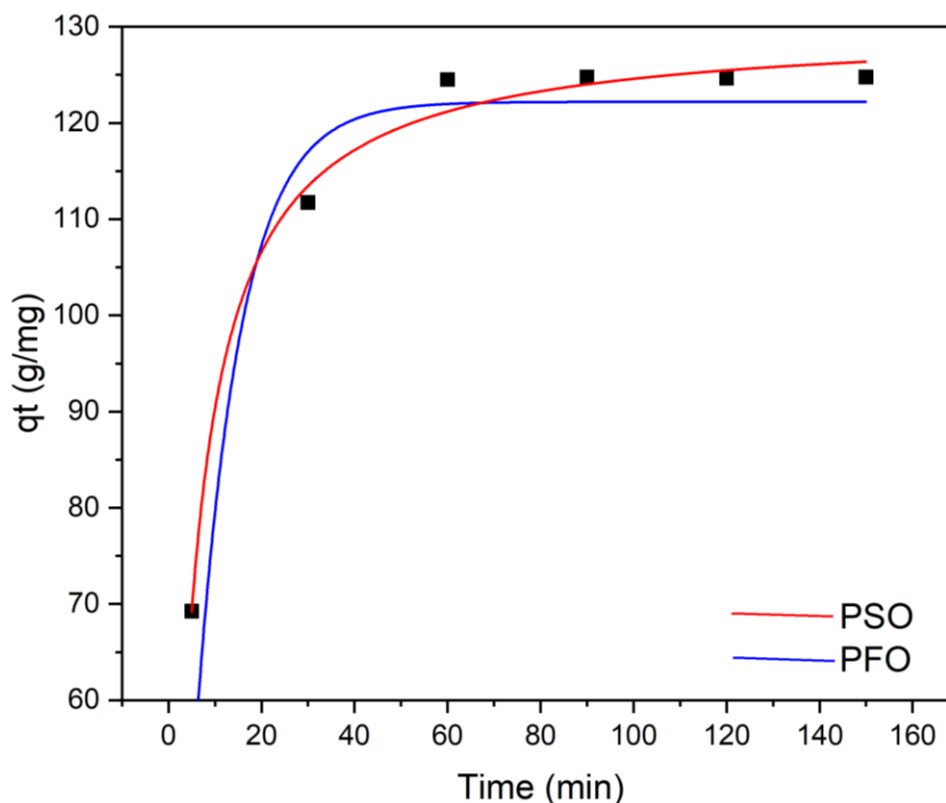


Figure 4. 19 Adsorption kinetic data of lead (II) ions.

Figure 4. 19 shows the adsorption kinetic of both pseudo-first-order and pseudo-second-order. By plotting the graph, the parameters such as  $k_1$ ,  $k_2$ ,  $q_e$ , and  $R^2$  could be obtained. The linear coefficient of the pseudo-second-order ( $R^2=0.99$ ) was higher than the pseudo-first-order kinetic model ( $R^2=0.79$ ). It indicated that the adsorption of lead(II) ions depends on the concentration of two molecules, which are  $Pb^{2+}$  and active sites of S-BSAC. The  $q_e$  from this model is 130.97 mg/g, close to the  $q_e$  of experimental data, which is 124.78 mg/g.

#### 4.2.6 Effect of pH

pH is an important parameter when studying the adsorption. This work conducted experiments using 20 mg S-BSAC in 25 mL of 100 mg/L of lead solution. The pH range in 3-6, and the experiments were performed at room temperature for 90 min. The results are shown in Figures 4. 20 and 4. 21.



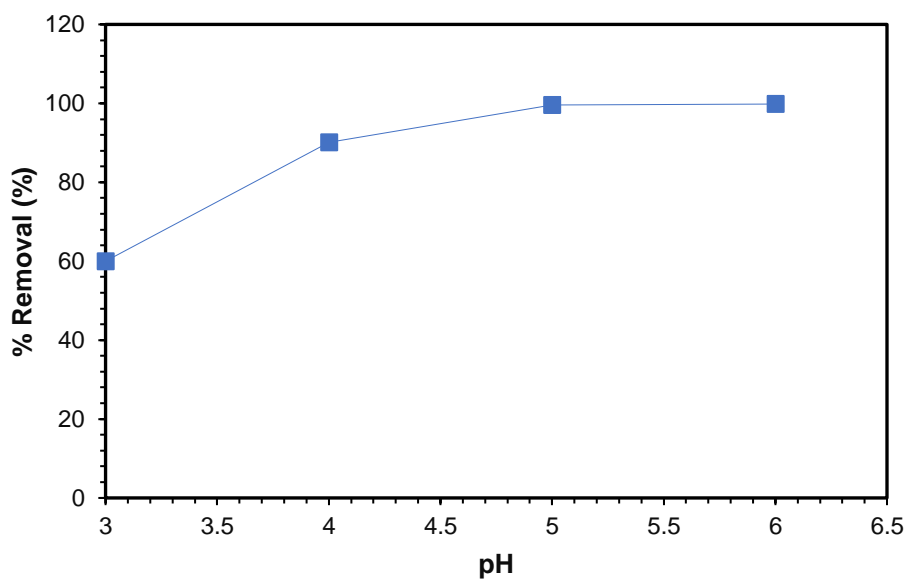


Figure 4. 20 Effect of pH on lead(II) ion removal efficiency of S-BSAC.

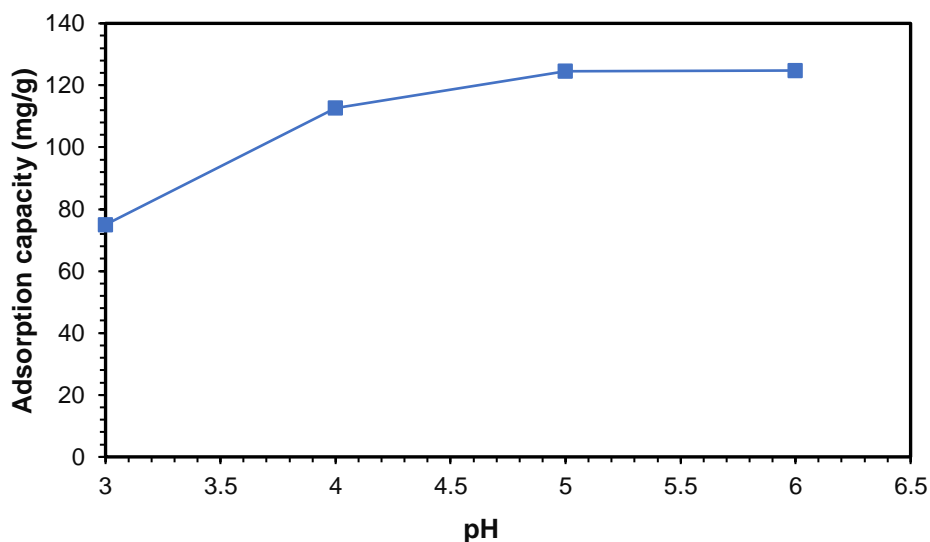


Figure 4. 21 Effect of pH on lead(II) ion adsorption capacity of S-BSAC.

Figures 4. 20, and 4. 21 show that the removal efficiency and adsorption capacity of S-BSAC increase with the increase in pH. At low pH, protons in acid solution ( $H^+$ ) can protonate binding sites of the chelating molecules. The surface of S-BSAC, rich in sulfur-containing groups, was in the protonated form of the corresponding functional groups. In other words, the number of positively charged

sites increased due to the protonation in an acidic environment. Thus, the lead(II) ions have to compete with protons ( $H^+$ ) to enter the sorbents' active site at low pH. The small size of the  $H^+$  ion makes it a strong competitor for this adsorption. As the pH increased, the solution became more basic, and sulfur-containing groups on the surface of S-BSAC were deprotonated and became more negatively charged, so the less number of competing protons for lead(II) ions adsorption on the active sites. With the increase of pH solution from 3 to 6, the adsorption capacity increased from 75.21 mg/g to 124.78 mg/g, and the removal efficiency increased from 60% to 99.82%. The highest adsorption capacity and removal efficiency were achieved at pH 6. If the pH is higher than 6, the result is unreliable due to the precipitation of lead(II) as  $Pb(OH)_2$ .

#### 4.2.7 Effect of adsorbent dosage

The adsorption efficiency of lead(II) ions with different adsorbent dosages was investigated. From Figure 4. 22, the removal rate of  $Pb^{2+}$  increased significantly as the dosage increased. When the dosage increased from 0.2 g/L to 0.8 g/L, the removal efficiency increased from 20% to 99.78%. This result may be ascribed to increased adsorption sites for lead(II) ions with increasing adsorbent dosage. When the dosage is greater than 1 g/L, the removal efficiency is limited, indicating that the adsorption dosage had a greater impact on removing lead(II) ions. The opposite situation occurs in the amount of metal ions adsorbed per weight unit of the adsorbents (Figure 4. 22), which could result from less contact between metal ions and per unit mass of the adsorbent. That is, more unoccupied active sites would no longer contribute to the adsorption process. Thus in this work, we select the optimum dosage of S-BSAC to be 0.8 g/L for the subsequent removal process.

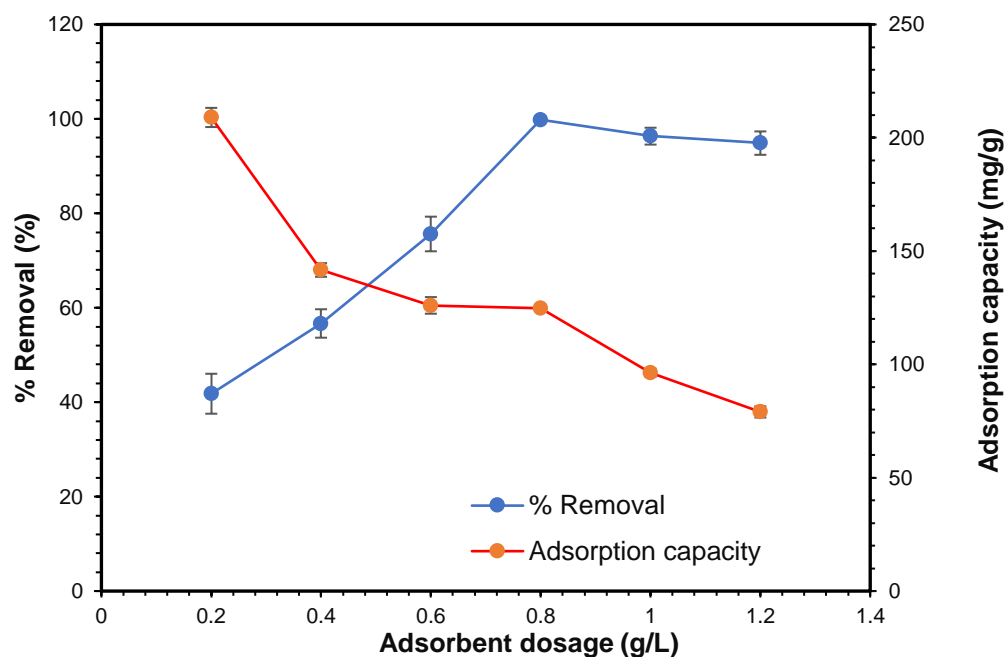


Figure 4. 22 Effect of adsorbent dosage on lead(II) ion removal efficiency and adsorption capacity of S-BSAC.

#### 4.2.8 Effect of co-existing cations

The influence of interfering cations on the selectivity of the adsorbent was investigated by introducing three metal ions ( $Mg^{2+}$ ,  $Cu^{2+}$ , and  $Zn^{2+}$ ) into the lead solutions. The impact of co-existing cations on the adsorption of  $Pb^{2+}$  ions was examined in 25 mL solutions containing 100 mg/L of mixed metal ions. As illustrated in Figure 4.23, the reduction in the quantity of  $Pb^{2+}$  ions in the presence of co-existing ions was comparatively lower than the decrease observed in the absence of co-existing ions (achieving a removal efficiency of 99.8%) within the solution. Both  $Mg^{2+}$  and  $Cu^{2+}$  are classified as hard and soft acids, and when these ions were mixed with the  $Pb^{2+}$  solution, the adsorption of lead(II) was high. This can be attributed to the relatively smaller number of hard and soft bases available on the surface of the activated carbon, which could bind with these acids. Another possible interaction mechanism was physical interaction through the pores of the activated carbon. On the other hand,  $Zn^{2+}$  and  $Pb^{2+}$  are categorized as borderline acids, leading to

competition for binding with the sulfur-containing groups (thiophene, sulfone and sulfide) present in the solution.

Consequently, the adsorption capacity for lead(II) ions significantly decreased when mixed with zinc(II) ions. However, the results still indicated that S-BSAC exhibited favorable selectivity for  $\text{Pb}^{2+}$  ions even in the presence of co-existing ions. Generally, the competitive adsorption ability varies among metal ions, potentially influenced by factors such as ion charges, molecular mass, and hydrated ionic radius. The co-existing cations compete with  $\text{Pb}^{2+}$  ions for active sites containing sulfur and oxygen-containing groups. Consequently, the number of active sites on the adsorbent's surface available for the adsorption of  $\text{Pb}^{2+}$  ions in the solution is reduced.

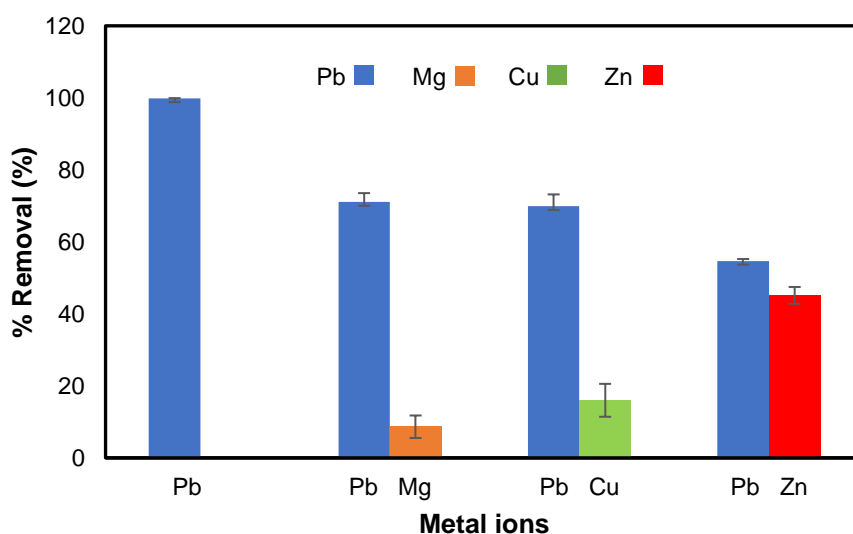
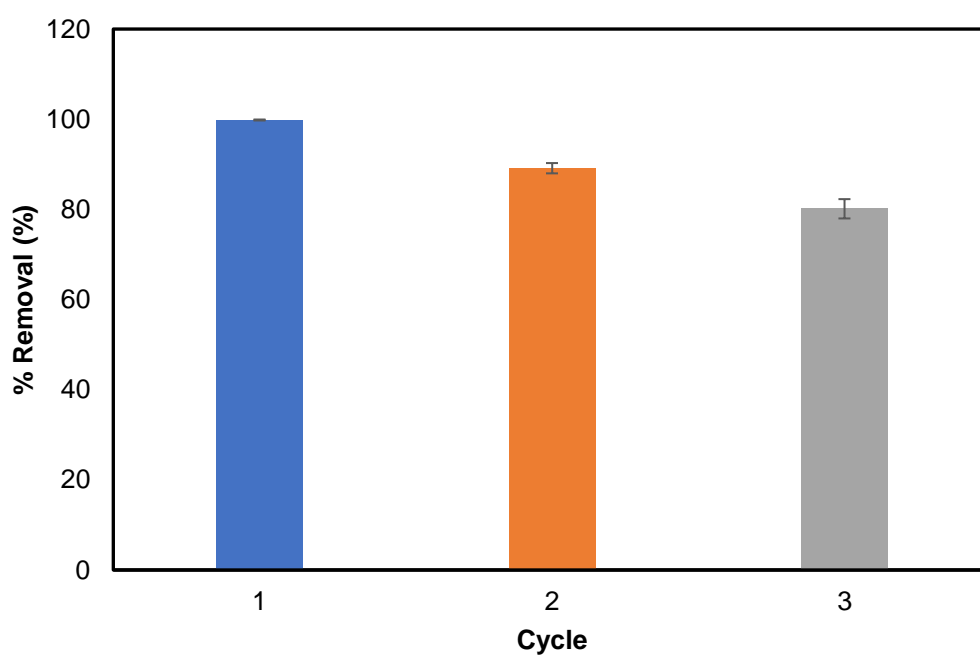


Figure 4. 23 Selective adsorption of Pb(II) on S-BSAC.

#### 4.2.9 Reusability of S-BSAC

Assessing the practical application potential of prepared adsorbents relies heavily on their reusability. To evaluate this factor, regenerative experiments were conducted using 1 M HCl as an eluting agent. The adsorption capacities of S-BSAC for  $\text{Pb}^{2+}$  were observed to remain above 85% even after three consecutive cycles of

adsorption and desorption, as depicted in Figure 4.24. This can be attributed to the strong affinity between S-BSAC and  $Pb^{2+}$ , which is likely due to the robust bonding ability between the metal ions and the sulfur-containing groups present on the surface of S-BSAC. Although HCl failed to completely desorb  $Pb^{2+}$  from the active sites on S-BSAC, the outcomes of the regeneration experiments indicate that S-BSAC can be repeatedly utilized as an effective adsorbent for practical wastewater treatment.



GHULALONGKORN UNIVERSITY  
Figure 4. 24 Reusability study of S-BSAC in 3 cycles.

## CHAPTER 5

### CONCLUSION

S-BSAC was prepared by one-step impregnation and pyrolysis of banana stem with sulfuric acid. The characterization of the material was done using XRD, SEM, surface area analyzer, and FTIR, confirming that the material was successfully prepared. The  $S_{\text{BET}}$  of the S-BSAC was 453.74 m<sup>2</sup>/g. The sulfur-containing groups attached to the surface of BSAC were based on the qualitative analysis using FTIR. The size of particles of S-BSAC were ranged from 70 - 100  $\mu\text{m}$ , as the banana stem was sieved in a 200 mesh sieve.

Adsorption studies of S-BSAC were investigated towards Pb<sup>2+</sup> in water. The behaviour of lead(II) removal mechanism predominantly through the chemical interaction, which is chelating of thiophene (C-S and Pb(II)), electrostatic interaction of sulfonate and sulfide and Pb (II), and this result agreed with the Langmuir isotherm and pseudo-second-order.

Table 5. 1 The adsorption behaviour of S-BSAC and optimal conditions for the removal of Pb<sup>2+</sup>

Parameters	Adsorption behaviours
Initial concentration to reach adsorption equilibrium (mg/L)	100
Adsorption isotherm	Langmuir isotherm
Time to reach adsorption equilibrium	90 min
Solution pH	6
Maximum adsorption capacity (mg/g)	126.85

This material's maximum adsorption capacity is lower than some reported results, as mentioned in the literature reviews session. This result could be happening due to

the biomass used as the source of carbon material affecting the surface area, which is quite low compared to other carbon sources.

#### Suggestions for further research

- Find the suitable condition to modify the BSAC.
- Optimize the preparation of activated carbon with some activating agents, the effect of time and temperature of pyrolysis.
- Investigate the effect of different eluent on the reusability of the S-BSAC for lead(II) removal.



## REFERENCES



จุฬาลงกรณ์มหาวิทยาลัย  
**CHULALONGKORN UNIVERSITY**



- [1] K. Raj and A. P. Das, "Environmental Chemistry and Ecotoxicology Lead pollution : Impact on environment and human health and approach for a sustainable solution," *Environ. Chem. Ecotoxicol.*, vol. 5, no. February, pp. 79–85, 2023, doi: 10.1016/j.enceco.2023.02.001.
- [2] M. R. Awual, M. M. Hasan, and H. Znad, "Organic-inorganic based nano-conjugate adsorbent for selective palladium(II) detection, separation and recovery," *Chem. Eng. J.*, vol. 259, pp. 611–619, Jan. 2015, doi: 10.1016/j.cej.2014.08.028.
- [3] G. A. Adebisi, Z. Z. Chowdhury, and P. A. Alaba, "Equilibrium, kinetic, and thermodynamic studies of lead ion and zinc ion adsorption from aqueous solution onto activated carbon prepared from palm oil mill effluent," *J. Clean. Prod.*, vol. 148, pp. 958–968, 2017, doi: 10.1016/j.jclepro.2017.02.047.
- [4] J. Bayuo, M. Rwiza, and K. Mtei, "A comprehensive review on the decontamination of lead(ii) from water and wastewater by low-cost biosorbents," *RSC Adv.*, vol. 12, no. 18, pp. 11233–11254, 2022, doi: 10.1039/d2ra00796g.
- [5] I. R. Chowdhury, S. Chowdhury, M. A. J. Mazumder, and A. Al-Ahmed, "Removal of lead ions (Pb<sup>2+</sup>) from water and wastewater: a review on the low-cost adsorbents," *Appl. Water Sci.*, vol. 12, no. 8, pp. 1–33, 2022, doi: 10.1007/s13201-022-01703-6.
- [6] M. S. Collin *et al.*, "Bioaccumulation of lead (Pb) and its effects on human: A review," *J. Hazard. Mater. Adv.*, vol. 7, no. March, p. 100094, 2022, doi: 10.1016/j.hazadv.2022.100094.
- [7] Y. Zhang and X. Duan, "Chemical precipitation of heavy metals from wastewater by using the synthetical magnesium hydroxy carbonate," *Water Sci. Technol.*, vol. 81, no. 6, pp. 1130–1136, 2020, doi: 10.2166/wst.2020.208.
- [8] M. M. Matlock, B. S. Howerton, and D. A. Atwood, "Chemical precipitation of lead from lead battery recycling plant wastewater," *Ind. Eng. Chem. Res.*, vol. 41, no. 6, pp. 1579–1582, 2002, doi: 10.1021/ie010800y.
- [9] Y. X. Liu, J. M. Yan, D. X. Yuan, Q. L. Li, and X. Y. Wu, "The study of lead removal from aqueous solution using an electrochemical method with a

- stainless steel net electrode coated with single wall carbon nanotubes," *Chem. Eng. J.*, vol. 218, pp. 81–88, 2013, doi: 10.1016/j.cej.2012.12.020.
- [10] Á. Golcs, L. Bezúr, P. Huszthy, and T. Tóth, "Liquid-liquid extraction and facilitated membrane transport of  $Pb^{2+}$  using a lipophilic acridono-crown ether as carrier," *J. Incl. Phenom. Macrocycl. Chem.*, vol. 99, no. 1–2, pp. 117–129, 2021, doi: 10.1007/s10847-020-01036-4.
- [11] J. Feng *et al.*, "The adsorption behavior and mechanism investigation of  $Pb(II)$  removal by flocculation using microbial flocculant GA1," *Bioresour. Technol.*, vol. 148, pp. 414–421, 2013, doi: 10.1016/j.biortech.2013.09.011.
- [12] M. Nemati, S. M. Hosseini, F. Parvizian, N. Rafiei, and B. Van der Bruggen, "Desalination and heavy metal ion removal from water by new ion exchange membrane modified by synthesized  $NiFe_2O_4/HAMPS$  nanocomposite," *Ionics (Kiel)*, vol. 25, no. 8, pp. 3847–3857, 2019, doi: 10.1007/s11581-019-02937-2.
- [13] M. Li, S. Kuang, Y. Kang, H. Ma, J. Dong, and Z. Guo, "Recent advances in application of iron-manganese oxide nanomaterials for removal of heavy metals in the aquatic environment," *Sci. Total Environ.*, vol. 819, p. 153157, 2022, doi: 10.1016/j.scitotenv.2022.153157.
- [14] S. Liu, S. Cui, H. Guo, Y. Wang, and Y. Zheng, "Adsorption of lead ion from wastewater using non-crystal hydrated calcium silicate gel," *Materials (Basel)*, vol. 14, no. 4, p. 842, 2021, doi: 10.3390/ma14040842.
- [15] M. S. Reza *et al.*, "Preparation of activated carbon from biomass and its' applications in water and gas purification, a review," *Arab J. Basic Appl. Sci.*, vol. 27, no. 1, pp. 208–238, 2020, doi: 10.1080/25765299.2020.1766799.
- [16] A. M. El-Wakil, S. M. Waly, W. M. Abou El-Maaty, M. M. Waly, M. Yilmaz, and F. S. Awad, "Triazine-Based Functionalized Activated Carbon Prepared from Water Hyacinth for the Removal of  $Hg^{2+}$ ,  $Pb^{2+}$ , and  $Cd^{2+}$  Ions from Water," *ACS Omega*, vol. 7, no. 7, pp. 6058–6069, 2022, doi: 10.1021/acsomega.1c06441.
- [17] L. Zhu, Y. Yao, D. Chen, and P. Lan, "The effective removal of  $Pb^{2+}$  by activated carbon fibers modified by l-cysteine: exploration of kinetics, thermodynamics and mechanism," *RSC Adv.*, vol. 12, no. 31, pp. 20062–20073, 2022, doi: 10.1039/d2ra01521h.

- [18] Q. Zuo, H. Zheng, P. Zhang, and Y. Zhang, "Functionalized Activated Carbon Fibers by Hydrogen Peroxide and Polydopamine for Efficient Trace Lead Removal from Drinking Water," *Langmuir*, vol. 38, no. 1, pp. 253–263, 2022, doi: 10.1021/acs.langmuir.1c02459.
- [19] Q. Zuo, H. Zheng, P. Zhang, and Y. Zhang, "Functionalized Activated Carbon Fibers by Hydrogen Peroxide and Polydopamine for Efficient Trace Lead Removal from Drinking Water," *Langmuir*, vol. 38, no. 1, pp. 253–263, 2022, doi: 10.1021/acs.langmuir.1c02459.
- [20] X. Liu, G. Li, C. Chen, X. Zhang, K. Zhou, and X. Long, "Banana stem and leaf biochar as an effective adsorbent for cadmium and lead in aqueous solution," *Sci. Rep.*, vol. 12, no. 1, pp. 1–14, 2022, doi: 10.1038/s41598-022-05652-7.
- [21] A. L. Wani, A. Ara, and J. A. Usmani, "Lead toxicity: A review," *Interdiscip. Toxicol.*, vol. 8, no. 2, pp. 55–64, 2015, doi: 10.1515/intox-2015-0009.
- [22] ITC News, "What are the world's favourite fruits?" <https://intracen.org/news-and-events/news/what-are-the-worlds-favourite-fruits> (accessed Apr. 04, 2023).
- [23] D. Reay, *Climate-Smart Food*. Springer International Publishing, 2019. doi: <https://doi.org/10.1007/978-3-030-18206-9>.
- [24] J. A. Ortiz-ulloa, M. F. Abril-gonzález, M. R. Pelaez-samaniego, and T. S. Zalamea-piedra, "Biomass yield and carbon abatement potential of banana crops ( *Musa* spp .) in Ecuador," pp. 18741–18753, 2021.
- [25] H. N. Chanakya and M. Sreesha, "Energy for Sustainable Development Anaerobic retting of banana and arecanut wastes in a plug flow digester for recovery of fiber , biogas and compost," *Energy Sustain. Dev.*, vol. 16, no. 2, pp. 231–235, 2012, doi: 10.1016/j.esd.2012.01.003.
- [26] B. F. Noeline, D. M. Manohar, and T. S. Anirudhan, "Kinetic and equilibrium modelling of lead(II) sorption from water and wastewater by polymerized banana stem in a batch reactor," *Sep. Purif. Technol.*, vol. 45, no. 2, pp. 131–140, 2005, doi: 10.1016/j.seppur.2005.03.004.
- [27] M. A. Al-Ghouti and D. A. Da'ana, "Guidelines for the use and interpretation of adsorption isotherm models: A review," *J. Hazard. Mater.*, vol. 393, no. January, p. 122383, 2020, doi: 10.1016/j.jhazmat.2020.122383.

- [28] H. Xu *et al.*, "Nanoporous activated carbon derived from rice husk for high performance supercapacitor," *J. Nanomater.*, vol. 2014, pp. 1–8, 2014, doi: 10.1155/2014/714010.
- [29] N. Rambabu, B. V. S. K. Rao, V. R. Surisetty, U. Das, and A. K. Dalai, "Production, characterization, and evaluation of activated carbons from de-oiled canola meal for environmental applications," *Ind. Crops Prod.*, vol. 65, pp. 572–581, 2015, doi: 10.1016/j.indcrop.2014.09.046.
- [30] Y. Huang and G. Zhao, "Preparation and characterization of activated carbon fibers from liquefied wood by KOH activation," *Holzforschung*, vol. 70, no. 3, pp. 195–202, 2016, doi: 10.1515/hf-2015-0051.
- [31] N. Khadhri, M. El Khames Saad, M. Ben Mosbah, and Y. Moussaoui, "Batch and continuous column adsorption of indigo carmine onto activated carbon derived from date palm petiole," *J. Environ. Chem. Eng.*, vol. 7, no. 1, p. 102775, 2019, doi: 10.1016/j.jece.2018.11.020.
- [32] V. O. Njoku, K. Y. Foo, M. Asif, and B. H. Hameed, "Preparation of activated carbons from rambutan (*Nephelium lappaceum*) peel by microwave-induced KOH activation for acid yellow 17 dye adsorption," *Chem. Eng. J.*, vol. 250, pp. 198–204, 2014, doi: 10.1016/j.cej.2014.03.115.
- [33] X. Feng, X. Ma, N. Li, C. Shang, X. Yang, and X. D. Chen, "Adsorption of quinoline from liquid hydrocarbons on graphite oxide and activated carbons," *RSC Adv.*, vol. 5, no. 91, pp. 74684–74691, 2015, doi: 10.1039/c5ra09228k.
- [34] A. Bhatnagar, W. Hogland, M. Marques, and M. Sillanpää, "An overview of the modification methods of activated carbon for its water treatment applications," *Chem. Eng. J.*, vol. 219, pp. 499–511, 2013, doi: 10.1016/j.cej.2012.12.038.
- [35] M. Yousefi *et al.*, "Modification of pumice with HCl and NaOH enhancing its fluoride adsorption capacity: Kinetic and isotherm studies," *Hum. Ecol. Risk Assess.*, vol. 25, no. 6, pp. 1508–1520, 2019, doi: 10.1080/10807039.2018.1469968.
- [36] L. F. Gleysteen and V. R. Deitz, "Hysteresis in the physical adsorption of nitrogen on bone char and other adsorbents," *J. Res. Natl. Bur. Stand. (1934)*,

- vol. 35, no. 4, p. 285, 1945, doi: 10.6028/jres.035.013.
- [37] J. Pallarés, A. González-Cencerrado, and I. Arauzo, "Production and characterization of activated carbon from barley straw by physical activation with carbon dioxide and steam," *Biomass and Bioenergy*, vol. 115, no. January, pp. 64–73, 2018, doi: 10.1016/j.biombioe.2018.04.015.
- [38] N. Byamba-Ochir, W. G. Shim, M. S. Balathanigaimani, and H. Moon, "Highly porous activated carbons prepared from carbon rich Mongolian anthracite by direct NaOH activation," *Appl. Surf. Sci.*, vol. 379, pp. 331–337, 2016, doi: 10.1016/j.apsusc.2016.04.082.
- [39] A. W. Samsuri, F. Sadegh-Zadeh, and B. J. Seh-Bardan, "Characterization of biochars produced from oil palm and rice husks and their adsorption capacities for heavy metals," *Int. J. Environ. Sci. Technol.*, vol. 11, no. 4, pp. 967–976, 2014, doi: 10.1007/s13762-013-0291-3.
- [40] M. Molina-Sabio and F. Rodriguez-Reinoso, "Role of chemical activation in the development of carbon porosity," *Colloids Surfaces A Physicochem. Eng. Asp.*, vol. 241, no. 1–3, pp. 15–25, 2004, doi: 10.1016/j.colsurfa.2004.04.007.
- [41] M. K. B. Gratuito, T. Panyathanmaporn, R. A. Chumnanklang, N. Sirinuntawittaya, and A. Dutta, "Production of activated carbon from coconut shell: Optimization using response surface methodology," *Bioresour. Technol.*, vol. 99, no. 11, pp. 4887–4895, 2008, doi: 10.1016/j.biortech.2007.09.042.
- [42] X. Y. Cui, F. Jia, Y. X. Chen, and J. Gan, "Influence of single-walled carbon nanotubes on microbial availability of phenanthrene in sediment," *Ecotoxicology*, vol. 20, no. 6, pp. 1277–1285, 2011, doi: 10.1007/s10646-011-0684-3.
- [43] B. Wang *et al.*, "Facile, low-cost, and sustainable preparation of hierarchical porous carbons from ion exchange resin: An improved potassium activation strategy," *Fuel*, vol. 179, pp. 274–280, 2016, doi: 10.1016/j.fuel.2016.03.088.
- [44] S. Yorgun, D. Yıldız, and Y. E. Şimşek, "Activated carbon from paulownia wood: Yields of chemical activation stages," *Energy Sources, Part A Recover. Util. Environ. Eff.*, vol. 38, no. 14, pp. 2035–2042, 2016, doi: 10.1080/15567036.2015.1030477.

- [45] M. Balajii and S. Niju, "Biochar-derived heterogeneous catalysts for biodiesel production," *Environ. Chem. Lett.*, vol. 17, no. 4, pp. 1447–1469, 2019, doi: 10.1007/s10311-019-00885-x.
- [46] N. Talreja, S. H. Jung, L. T. H. Yen, and T. Y. Kim, "Phenol-formaldehyde-resin-based activated carbons with controlled pore size distribution for high-performance supercapacitors," *Chem. Eng. J.*, vol. 379, no. June 2019, pp. 1–10, 2020, doi: 10.1016/j.cej.2019.122332.
- [47] P. Zhang *et al.*, "Ultramicroporous carbons with extremely narrow pore size distribution via in-situ ionic activation for efficient gas-mixture separation," *Chem. Eng. J.*, vol. 375, no. June, 2019, doi: 10.1016/j.cej.2019.121931.
- [48] M. Mariana *et al.*, "Recent advances in activated carbon modification techniques for enhanced heavy metal adsorption," *J. Water Process Eng.*, vol. 43, no. June, p. 102221, 2021, doi: 10.1016/j.jwpe.2021.102221.
- [49] R. G. Pearson, "Recent advances in the concept of hard and soft acids and bases," *J. Chem. Educ.*, vol. 64, no. 7, pp. 561–567, 1987, doi: 10.1021/ed064p561.
- [50] S. Baytak, Z. Arslan, U. States, and G. Survey, "Solid Phase Extraction of Trace Elements in Water and Tissue Samples on a Mini Column with Diphenylcarbazone Impregnated Nano-TiO<sub>2</sub> and Their Determination by Inductively Coupled Plasma Optical Emission Spectrometry," *CLEAN - Soil Air Water*, vol. 43, no. February, pp. 822–829, 2015, doi: 10.1002/clen.201400348.
- [51] X. Chen *et al.*, "Isotherm models for adsorption of heavy metals from water - A review," *Chemosphere*, vol. 307, no. P1, p. 135545, 2022, doi: 10.1016/j.chemosphere.2022.135545.
- [52] M. S. Ismail, M. D. Yahya, M. Auta, and K. S. Obayomi, "Facile preparation of amine -functionalized corn husk derived activated carbon for effective removal of selected heavy metals from battery recycling wastewater," *Heliyon*, vol. 8, no. 5, p. e09516, 2022, doi: 10.1016/j.heliyon.2022.e09516.
- [53] N. Tang *et al.*, "Efficient removal of Cd<sup>2+</sup> and Pb<sup>2+</sup> from aqueous solution with amino- and thiol-functionalized activated carbon: Isotherm and kinetics modeling," *Sci. Total Environ.*, vol. 635, pp. 1331–1344, 2018, doi:

- 10.1016/j.scitotenv.2018.04.236.
- [54] S. M. Waly, A. M. El-Wakil, W. M. A. El-Maaty, and F. S. Awad, "Efficient removal of Pb(II) and Hg(II) ions from aqueous solution by amine and thiol modified activated carbon," *J. Saudi Chem. Soc.*, vol. 25, no. 8, p. 101296, Aug. 2021, doi: 10.1016/j.jscs.2021.101296.
- [55] D. Lv *et al.*, "Application of EDTA-functionalized bamboo activated carbon (BAC) for Pb(II) and Cu(II) removal from aqueous solutions," *Appl. Surf. Sci.*, vol. 428, pp. 648–658, 2018, doi: 10.1016/j.apsusc.2017.09.151.
- [56] A. Chatla *et al.*, "Influence of calcination atmosphere on Fe doped activated carbon for the application of lead removal from water," *Colloids Surfaces A Physicochem. Eng. Asp.*, vol. 652, no. July, p. 129928, 2022, doi: 10.1016/j.colsurfa.2022.129928.
- [57] M. S. Adly, S. M. El-Dafrawy, A. A. Ibrahim, S. A. El-Hakam, and M. S. El-Shall, "Efficient removal of heavy metals from polluted water with high selectivity for Hg(ii) and Pb(ii) by a 2-imino-4-thiobiuret chemically modified MIL-125 metal-organic framework," *RSC Adv.*, vol. 11, no. 23, 2021, doi: 10.1039/d1ra00927c.
- [58] S. M. Waly, A. M. El-Wakil, W. M. A. El-Maaty, and F. S. Awad, "Efficient removal of Pb(II) and Hg(II) ions from aqueous solution by amine and thiol modified activated carbon," *J. Saudi Chem. Soc.*, vol. 25, no. 8, pp. 1–11, 2021, doi: 10.1016/j.jscs.2021.101296.
- [59] W. S. Chen, Y. C. Chen, and C. H. Lee, "Modified Activated Carbon for Copper Ion Removal from Aqueous Solution," *Processes*, vol. 10, no. 1, 2022, doi: 10.3390/pr10010150.
- [60] S. Zhang *et al.*, "Polyaniline nanorods dotted on graphene oxide nanosheets as a novel super adsorbent for Cr(vi)," *J. Chem. Soc. Dalt. Trans.*, vol. 42, no. 22, pp. 7854–7858, 2013, doi: 10.1039/c3dt50149c.
- [61] M. S. Alhumaimess, "Sulfhydryl functionalized activated carbon for Pb(II) ions removal: kinetics, isotherms, and mechanism," *Sep. Sci. Technol.*, vol. 55, no. 7, pp. 1303–1316, 2020, doi: 10.1080/01496395.2019.1589513.
- [62] H. L. Ma *et al.*, "Functionalization and reduction of graphene oxide with p-phenylene diamine for electrically conductive and thermally stable

polystyrene composites," *ACS Appl. Mater. Interfaces*, vol. 4, no. 4, pp. 1948–1953, 2012, doi: 10.1021/am201654b.

- [63] M. Deng, Y. Huang, X. Zhang, Z. Feng, J. Gou, and B. Sun, "Preparation of a novel chelating resin bearing amidinothiourea moieties and its removal properties for Hg(II) ions in aqueous solution," *Sep. Sci. Technol.*, vol. 51, no. 9, pp. 1499–1508, Jun. 2016, doi: 10.1080/01496395.2016.1166135.





## VITA

NAME Imelda Octa Tampubolon

DATE OF BIRTH 29 October 1991

PLACE OF BIRTH Pematangsiantar

INSTITUTIONS ATTENDED Chulalongkorn University

HOME ADDRESS Diana Court, 9 Phetchaburi road soi 6, Thanon  
Phetchaburi, Bangkok

